20,000 *g* for 2 min at −9°C. To determine the concentration of ATP and its degradation products, the supernatant of the homogenate was neutralized with a solution of 2 N KOH and 0.4 M imidazole and then centrifuged at 20,000 *g* for 2 min at −9°C. The supernatant was filtered through a 0.45-μm pore Cosmonice filter W (Nacalai Tesque) and then analyzed by HPLC (DX300, Dionex, Sunnyvale, CA) equipped with an SPD-10Ai detector (Shimadzu, Kyoto, Japan) and an AS-8020 autoinjector (Tosho, Tokyo, Japan). The filtrate was applied to a COSMOSIL 5PE-MS Packed Column (4.6 × 250 mm; Nacalai Tesque) equilibrated with 20 mM sodium phosphate containing 25 mM *N,N*-diethylethanolamine at 1 ml/min. Elution was monitored at 254 nm.

3-MG transport. To assay 3-MG transport, muscles were transferred to 2 ml of KRB containing 1 mM [^{3}H]3-MG (1.5 μCi/ml) and 7 mM D-[1-^{14}C]mannitol (0.3 μCi/ml) at 30°C and further incubated for 10 min (21). The muscles were then blotted onto filter paper, trimmed, frozen in liquid nitrogen, and stored at −80°C. Frozen muscles were weighed and processed by incubating them in 300 μl of 1 M NaOH at 80°C for 10 min. Digestates were neutralized with 300 μl of 1 M HCl, and particulates were precipitated by centrifugation at 20,000 *g* for 2 min. Radioactivity in aliquots of the digested protein was determined by liquid scintillation counting for dual labels, and the extracellular and intracellular spaces were calculated.

Statistical analysis. Results are presented as means ± SE. Means were compared by one-way analysis of variance followed by post hoc comparison with Dunnett's or Scheffé's test as appropriate. Unpaired *t*-tests were used for comparison as appropriate.

RESULTS

AMPKα1 activity was elevated immediately after isolation and decreased during incubation. To allow the epitrochlearis muscles to recover from the isolating procedure, we first determined the incubation period that stabilizes AMPK activity, as measured in anti-α1 and anti-α2 immunoprecipitates from muscles that had been either frozen immediately after isolation or incubated in KRBP for 60, 100, or 120 min and then frozen. AMPKα1 kinase activity was lower in the incubated muscle than in muscle frozen immediately after isolation (Fig. 1*A*). AMPKα1 activity attained a constant level at 60 min of incubation and did not change afterwards, whereas AMPKα2 activity remained unchanged throughout the incubation period (Fig. 1*A*). We also investigated whether AMPKα1 activity differs between muscles frozen immediately after isolation under anesthesia and muscles incubated for 100 min. Regardless of whether cervical dislocation was or was not performed, AMPKα1 activity was higher in the muscles frozen immediately after isolation under anesthesia than in the incubated muscles; AMPKα2 activity did not differ between conditions (Fig. 1*B*).

ES increased AMPKα1activity in a time- and frequency-dependent manner. Tetanic contraction is a standard procedure to stimulate AMPK activity in isolated skeletal muscle (21, 35). Even a single 10-s tetanic contraction is enough to activate

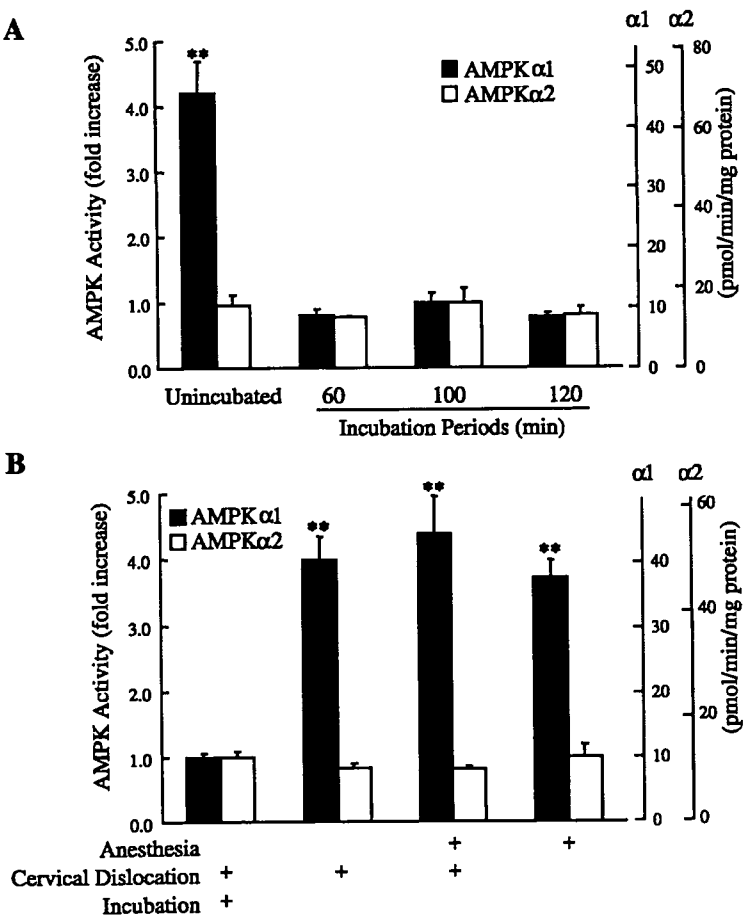

Fig. 1. Incubation decreases 5′-AMP-activated protein kinase (AMPK)α1 activity to a constant level in isolated rat epitrochlearis muscles. *A*: rats were killed by cervical dislocation, and isolated muscles were either frozen immediately after isolation or incubated in Krebs-Ringer bicarbonate buffer containing 2 mM pyruvate (KRBP) for 60, 100, or 120 min and then frozen in liquid nitrogen. *B*: rats were randomly assigned to an anesthetized or a nonanesthetized group. In the anesthetized group, rats were anesthetized with pentobarbital sodium (50 mg/kg body wt ip), and muscles were isolated with or without cervical dislocation. Isolated muscles were frozen immediately after isolation. In the nonanesthetized group, rats were killed by cervical dislocation, and isolated muscles were frozen immediately after isolation or incubated in KRBP for 100 min and then frozen in liquid nitrogen. Isoform-specific AMPK activity was determined in the anti-α1 or anti-α2 subunit of AMPK immunoprecipitates. Fold increases are expressed relative to the activity of muscles incubated for 100 min. Values are means ± SE; $n = 6$ per group. $^{**}P < 0.01$ vs. 100-min incubation group.

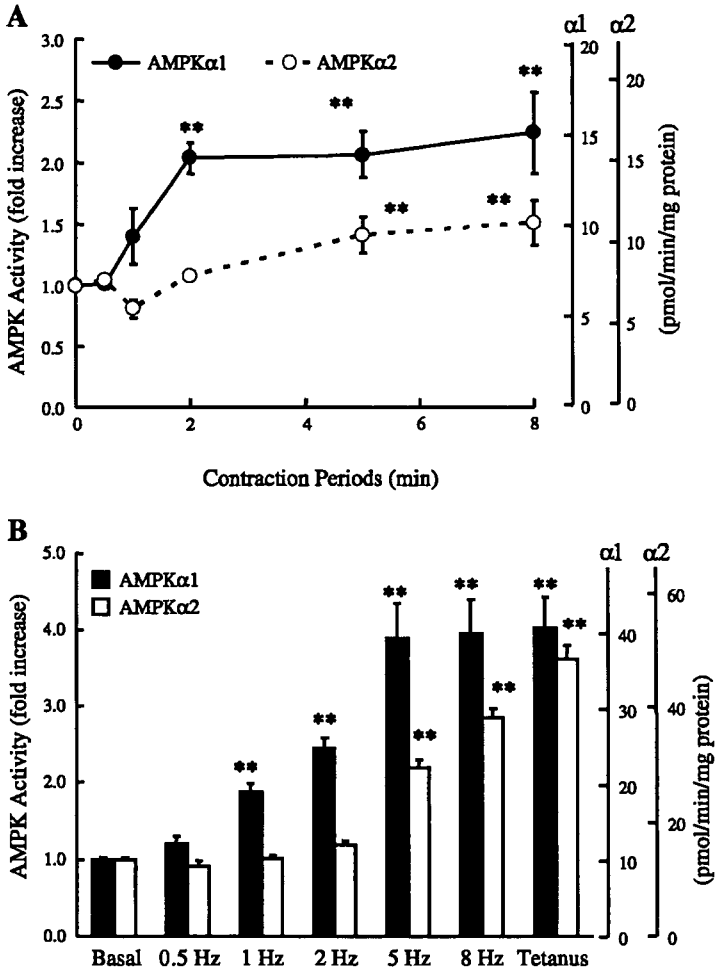

Fig. 2. Low-frequency electrical stimulation (ES) increases predominantly AMPKα1 activity in a time- and contraction frequency-dependent manner in rat epitrochlearis muscles. Isolated muscles were electrically stimulated (50 V) to contract at 1 Hz for the indicated periods (*A*) or at the frequencies indicated for 2 min (*B*). To tetanically contract the muscles, muscles were stimulated for 10 s/min, repeated 10 times. Isoform-specific AMPK activity was determined in anti-α1 or anti-α2 subunit of AMPK immunoprecipitates. Values are means ± SE; n = 9–29 per group. $^{**}P < 0.01$ vs. the 0-min (*A*) or vs. the 0-Hz group (*B*).

both AMPKα1 and AMPKα2 (35). To investigate the time dependency of isoform-specific AMPK activity stimulated by ES at frequencies lower than the tetanic stimulus (100 Hz), isolated epitrochlearis muscles were incubated to stabilize AMPK activity and then stimulated at 1 Hz for various periods. ES at 1 Hz rapidly activated AMPKα1 twofold within 2 min and maintained maximal activity for 2–8 min (Fig. 2*A*). In contrast, AMPKα2 activation required ≥5 min of ES, and the 1.5-fold increase was smaller than that of AMPKα1 ($P < 0.05$; Fig. 2*A*). To determine whether this effect was dependent on stimulation frequency, isolated epitrochlearis muscles were stimulated for 2 min at various frequencies. ES at 1 and 2 Hz activated predominantly AMPKα1, whereas ES at 5 and 8 Hz activated both AMPKα1 and AMPKα2 (Fig. 2*B*). ES at 5 and 8 Hz activated AMPKα1 maximally and to the same degree as tetanic contraction did, about four times the basal level, whereas the activity of AMPKα2 was less than the maximal level achieved at 8 Hz (Fig. 2*B*).

The primary site responsible for AMPK activation is the Thr^{172} residue in both the α1 and α2 catalytic subunits (17, 43). To determine whether the ES-induced activation at 1 and 2 Hz of predominantly AMPKα1 was accompanied by the phosphorylation of Thr^{172}, we measured the degree of phosphorylation of Thr^{172} by use of a phosphospecific antibody in homogenates from muscles that had been stimulated by ES at the two frequencies. Compared with sham-operated muscles, muscles simulated with ES at 1 and 2 Hz exhibited markedly increased phosphorylation of Thr^{172} (Fig. 3).

ES at 1 and 2 Hz changed neither AMP nor the AMP/ATP ratio. To determine whether ES-induced activation of AMPKα1 results from the conventional changes associated with increased AMPK activity (33), we measured AMP concentration and the AMP/ATP ratio after stimulation. ES at 1 and 2 Hz, which activated AMPKα1 but not AMPKα2, did not increase AMP concentration or the AMP/ATP ratio (Fig. 4, *A* and *B*). In contrast, ES at 5 and 8 Hz, and tetanic stimulation, which activated both AMPKα1 and AMPKα2, markedly increased AMP concentration and the AMP/ATP ratio (Fig. 4, *A* and *B*).

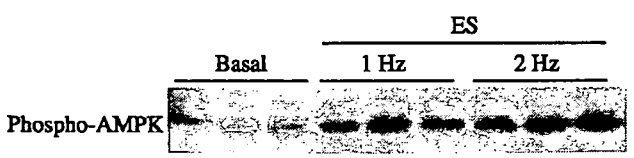

Fig. 3. Low-frequency ES increases phosphorylation of Thr^{172} in the AMPK α-subunit. Isolated muscles were electrically stimulated (50 V) to contract at 1 and 2 Hz for 2 min, and cell lysates were subjected to Western blot analysis with an anti-phosphorylated AMPK antibody.

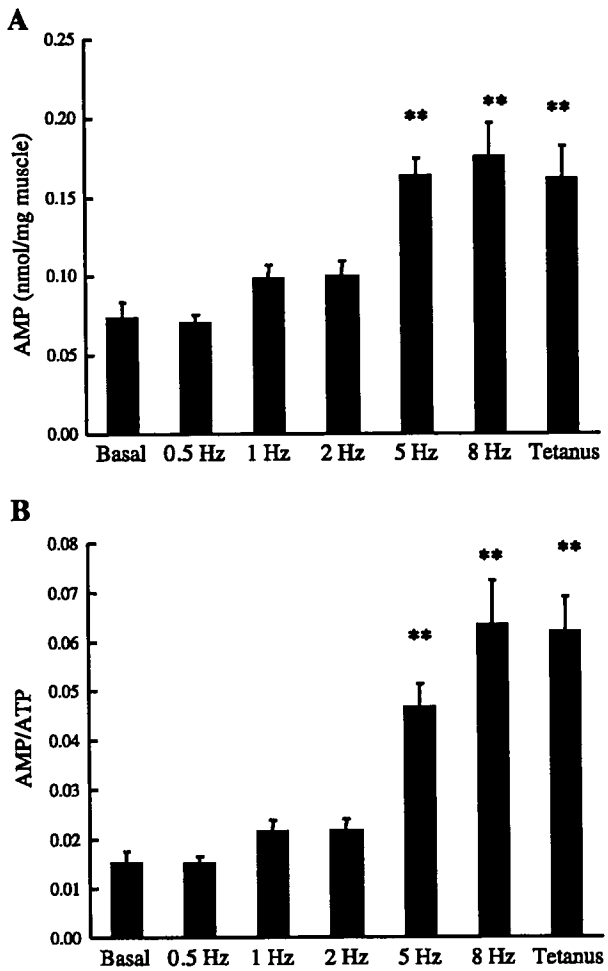

Fig. 4. Adenine nucleotide levels in epitrochlearis muscles treated with low-frequency ES. Isolated muscles were electrically stimulated (50 V) to contract for 2 min at the frequencies indicated. To tetanically contract the muscles, muscles were stimulated for 10 s/min, repeated 10 times. Intracellular AMP concentration (*A*) and ATP concentration were determined by HPLC, and the AMP/ATP ratio (*B*) were calculated. Values are means ± SE; $n = 8$–9 per group. $^{**}P < 0.01$ vs. basal values.

Predominant activation of AMPKα1 by ES at 1 and 2 Hz was associated with increased 3-MG transport and ACC phosphorylation. We next investigated whether ES at 1 and 2 Hz acutely affects glucose transport activity and the phosphorylation state of ACC, a downstream target of AMPK, in skeletal muscle. ES at 1 and 2 Hz increased the transport of the nonmetabolizable glucose analog 3-MG in a frequency-dependent manner (Fig. 5). We used a phosphospecific antibody that recognizes rat ACC1 phosphorylated at Ser^{79} to assess the specific phosphorylation of skeletal muscle ACC, because this site is equivalent to Ser^{79} of ACC1 (15, 37). ES at 1 and 2 Hz increased glucose transport and ACC phosphorylation (Fig. 6).

DISCUSSION

Our data show three novel findings relating to the isoform-specific AMPK profile in skeletal muscle. First, immediately after isolation, the activity of AMPKα1 increased greatly but the activity of AMPKα2 did not change (Fig. 1, *A* and *B*).

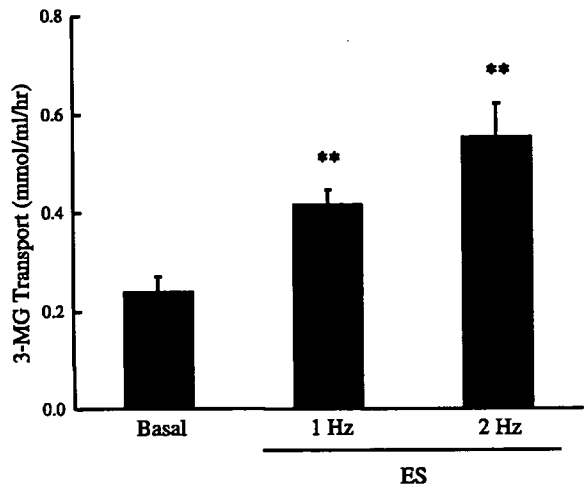

Fig. 5. Electrical stimulation increases 3-*O*-methyl-D-glucose (3-MG) transport in rat epitrochlearis muscles. Isolated muscles were electrically stimulated (1 or 2 Hz at 50 V) to contract for 2 min. Values are means ± SE; $n = 6$–10 per group. $^{**}P < 0.01$ vs. basal values.

Second, muscle contraction induced by ES at 1 and 2 Hz for 2 min activated AMPKα1 but not AMPKα2 (Fig. 2*B*), suggesting that AMPKα1 is more sensitive to low-intensity contraction than AMPKα2 is. Third, contraction-induced AMPKα1 activation was associated with increased glucose transport and ACC phosphorylation (Figs. 5 and 6).

We believe that the marked activation of AMPKα1 immediately after isolation is a post mortem artifact, on the basis of previous studies of liver AMPK (8, 14, 33) showing that, in liver dissected at ambient temperature, 3-hydroxy-3-methylglutaryl-CoA (HMG-CoA) reductase, one of the downstream targets of AMPK, is highly phosphorylated and inactivated (8). In contrast, in liver dissected after cold clamping and homogenized within 10 s after dissection, most HMG-CoA reductase is in an unphosphorylated active form (8), indicating that liver AMPK remains inactive in vivo and is easily activated as a post mortem artifact. Moreover, in freshly isolated rat hepatocytes, AMPK activity increases and then decreases to the expected in vivo level during incubation in oxygenated medium for 60 min (33). Hardie and Carling (14) proposed that rapid cooling is required to preserve the in vivo activation state of AMPK and that incubation in oxygenated medium restores AMPK activity to in vivo levels. Consistent with this proposal, AMPKα1 activation is not observed in muscle after electrically stimulated in situ contraction followed by muscle isolation (40, 46). In contrast, AMPKα1 activation occurs in muscle after electrically stimulated in situ contraction followed by freeze clamping (24).

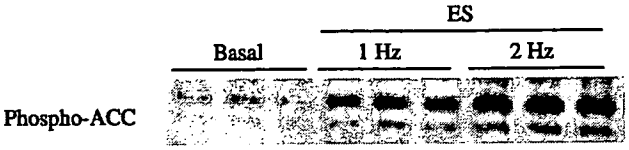

Fig. 6. Low-frequency ES increases phosphorylation of serine in acetyl-CoA carboxylase (ACC). Isolated muscles were electrically stimulated (50 V) to contract at 1 or 2 Hz for 2 min, and cell lysates were subjected to Western blot analysis with an anti-phosphorylated ACC antibody.

We have not identified the critical step of AMPKα1 activation induced by our isolation procedure. Ischemia limits oxygen supply and leads to reduced ATP generation and can activate AMPK (20), and stopping or reducing the blood or oxygen supply to muscles during isolation is one possible cause of AMPKα1 activation. However, hypoxic energy deprivation should activate both AMPKα1 and AMPKα2 (20). In addition, the time needed to freeze the muscle after cervical dislocation was about 30 s, which was about the same amount of time needed to freeze the tissue incubated in oxygenated buffer and then exposed to room air. Furthermore, the activation of AMPKα1 by muscle isolation under anesthesia without cervical dislocation (Fig. 1*B*) shows clearly that cervical dislocation is not a critical step in the activation of AMPKα1. The freezing procedure after incubation is nearly identical to that used after isolation. Thus changes in unidentified factors, such as nervous system input or a soluble factor, might cause the post mortem artifact and increase skeletal muscle AMPKα1 activation during the isolation procedures.

Our finding that low-intensity contraction of skeletal muscle activated mainly AMPKα1 differs from that of previous studies showing predominantly AMPKα2 activation (12, 44, 50). Our use of a different muscle preparation might explain these differences. We measured the AMPK activity of muscles that had been isolated, incubated in KRBP, and then stimulated to contract, whereas previous studies measured AMPK activity of muscles isolated after contraction (12, 44, 50). Because isolation can activate AMPKα1, the actual contraction-induced increase of AMPKα1 activity would not be apparent in the latter protocol. AMPKα1 could also be activated by isolation of both contracted and noncontracted muscles. Our incubation for more than 60 min decreased AMPKα1 activity to a constant level and allowed us to observe the activation of AMPKα1 in low-intensity stimulated contracted muscle.

The finding that AMPKα1 activation was not accompanied by an increase in AMP concentration and the AMP/ATP ratio (Fig. 4, *A* and *B*) suggests that AMPKα1 activation induced by low-intensity contraction is regulated by an AMP-independent mechanism. Although intracellular energy status is an important determinant of AMPK activity (1, 2, 9, 33, 39), recent studies have shown that AMPK is activated by phosphorylation in the absence of changes in the concentration of AMP or ATP or in ADP/ATP or AMP/ATP ratios (11, 22, 32, 45, 51). Our data (Fig. 4) and those of others (22, 45) are consistent in showing that the predominant activation of AMPKα1 is not accompanied by a decrease in intracellular energy status in skeletal muscle. SNP activates AMPKα1 in extensor digitorum longus muscle without depleting ATP (22), and H_2O_2 activates AMPKα1 in rat epitrochlearis muscle without increasing AMP concentration and the AMP/ATP ratio (45). We cannot exclude the possibility that AMPKα1 is activated by the increase in free AMP content, which comprises 0.11–0.50% of the total AMP content (13) and increases markedly in response to muscle contraction (7, 25). Importantly, however, a study using purified AMPK showed that AMPKα2 depends more on AMP activation by the upstream kinase than does AMPKα1 (41). In this context, the absence of AMPKα2 activation in our study also suggests that AMP does not accumulate in muscle and that AMPKα1 activation involves an AMP-independent mechanism (Fig. 2, *A* and *B*). Moreover, we detected parallel increases in AMP concentration and AMPKα2 activity in muscles stimulated by ES at ≥5 Hz (Figs. 2*B* and 4*A*).

Our finding that the predominant AMPKα1 activation is accompanied by phosphorylation of the α-subunit in Thr^{172} suggests that an upstream kinase is involved in AMPKα1 activation by low-intensity contracted muscle (Fig. 3). Two mammalian AMPKKs have been identified: Ca^{2+}/calmodulin-dependent protein kinase kinase (CaMKK) (19, 23) and the LKB1 complex consisting of LKB1 and two regulatory proteins, called Ste20-related adaptor protein and mouse protein 25 (16). In vitro studies have demonstrated that CaMKK is activated by Ca^{2+} and calmodulin but not by AMP (19). In an LKB1-deficient cell line, AMPK can be activated by treatment with mannitol, 2-deoxyglucose, and the Ca^{2+} ionophore ionomycin, but not by the AMP analog AICAR (23). In rat brain slices, depolarization induced by increasing K^+ concentration increases intracellular Ca^{2+} concentration by opening the voltage-gated Ca^{2+} channel and activates AMPK without elevating the AMP/ATP ratio; this activation is blocked by the CaMKK inhibitor STO-609 (18). AMP concentration did not increase in muscles stimulated by ES at 1 and 2 Hz (Fig. 4), suggesting that CaMKK might be responsible for the predominant activation of AMPKα1. In contrast, the LKB1 complex is constitutively active and is not directly activated by AMP, but the binding of AMP to AMPK facilitates the phosphorylation of AMPK by the LKB1 complex (16, 40). Thus the LKB1 complex may depend more on AMP to phosphorylate AMPK than does CaMKK. We cannot discount the possible involvement of yet-to-be-characterized AMPKKs, and further study is needed to clarify the AMPKK that activates predominantly AMPKα1 in low-intensity contracting skeletal muscle.

Our results show that ES at 1 and 2 Hz activates AMPKα1 and increases in the rate of glucose transport and ACC phosphorylation, indicating that AMPKα1, as well as AMPKα2, is involved in contraction-stimulated glucose transport and ACC phosphorylation. Our results are consistent with previous studies showing that low-intensity muscle contraction increases glucose transport and ACC phosphorylation (30, 37). ES at 1 and 2.5 Hz for 5 min increases glucose transport in isolated rat soleus muscles (30). ACC activity decreases after in situ contraction of rat gastrocnemius muscle stimulated by ES at 0.2 and 1 Hz for 5 min via the tibial nerve, and this decreased activity is inversely correlated with the concentration of phosphorylated ACC (37). Moreover, H_2O_2 activates increased glucose transport and ACC phosphorylation associated with AMPKα1 activation (45). SNP increases glucose transport associated with AMPKα1 activation (22). In support of our observations, contraction-induced glucose transport is not reduced by knockout of the α1- or α2-subunit of AMPK but is inhibited by dominant mutants of both isoforms (27, 34).

Our results lead us to hypothesize that *1*) AMPKα1 regulation is more sensitive to physical or physiological stress than AMPKα2 is; *2*) AMPKα1 is the predominant isoform activated by low-intensity contractions; *3*) AMPKα1 activation induced by low-intensity contractions is regulated by an AMP-independent phosphorylation, whereas AMPKα2 activation induced by high-intensity contraction is regulated by AMP-dependent mechanism; and *4*) activation of each isoform enhances glucose transport and ACC phosphorylation in skeletal muscle. Previous data show that low-intensity exercise, even at a level (e.g., 30–40% of $\dot{V}O_{2max}$) previously believed not to activate

AMPK, increases skeletal muscle glucose transport and ACC phosphorylation (4, 28), suggesting the involvement of an AMPK-independent pathway. Our results suggest that AMPKα1 may be activated in these muscles by low-intensity exercise and that measuring the activity may be disturbed by additional activation during isolation. Only during very-high-intensity exercise, when the activation by muscle contraction may exceed that of the isolating stimuli, would AMPKα1 activity be detectable.

In summary, we have demonstrated for the first time that muscle AMPKα1, but not AMPKα2, is activated immediately after isolation. Stabilizing muscle in KRBP followed by low-intensity contraction activates AMPKα1 via phosphorylation without increasing AMP concentration, and it increases glucose transport and ACC phosphorylation. We conclude that low-intensity muscle contraction activates AMPKα1 and leads to enhanced glucose transport and ACC phosphorylation in rat skeletal muscle.

ACKNOWLEDGMENTS

We thank Akira Otaka for providing the purified SAMS peptide and isoform-specific antigen peptides. We are grateful to Kazuo Inoue and Teruo Kawada for suggestions, and to Chikako Wada for secretarial assistance. We also thank the Radioisotope Research Center, Kyoto University, for instrumental support in radioisotope experiments.

GRANTS

This work was supported by research grants from the Japanese Ministry of Education, Science, Sports, and Culture (to T. Hayashi). T. Toyoda was supported by a Research Fellowship of the Japan Society for the Promotion of Science for Young Scientists.

REFERENCES

1. **Carling D, Clarke PR, Zammit VA, and Hardie DG.** Purification and characterization of the AMP-activated protein kinase. Copurification of acetyl-CoA carboxylase kinase and 3-hydroxy-3-methylglutaryl-CoA reductase kinase activities. *Eur J Biochem* 186: 129–136, 1989.
2. **Carling D, Zammit VA, and Hardie DG.** A common bicyclic protein kinase cascade inactivates the regulatory enzymes of fatty acid and cholesterol biosynthesis. *FEBS Lett* 223: 217–222, 1987.
3. **Chen ZP, McConell GK, Michell BJ, Snow RJ, Canny BJ, and Kemp BE.** AMPK signaling in contracting human skeletal muscle: acetyl-CoA carboxylase and NO synthase phosphorylation. *Am J Physiol Endocrinol Metab* 279: E1202–E1206, 2000.
4. **Chen ZP, Stephens TJ, Murthy S, Canny BJ, Hargreaves M, Witters LA, Kemp BE, and McConell GK.** Effect of exercise intensity on skeletal muscle AMPK signaling in humans. *Diabetes* 52: 2205–2212, 2003.
5. **Clark SA, Chen ZP, Murphy KT, Aughey RJ, McKenna MJ, Kemp BE, and Hawley JA.** Intensified exercise training does not alter AMPK signaling in human skeletal muscle. *Am J Physiol Endocrinol Metab* 286: E737–E743, 2004.
6. **Davies SP, Hawley SA, Woods A, Carling D, Haystead TA, and Hardie DG.** Purification of the AMP-activated protein kinase on ATP-gamma-sepharose and analysis of its subunit structure. *Eur J Biochem* 223: 351–357, 1994.
7. **Dudley GA and Terjung RL.** Influence of acidosis on AMP deaminase activity in contracting fast-twitch muscle. *Am J Physiol Cell Physiol* 248: C43–C50, 1985.
8. **Easom RA and Zammit VA.** A cold-clamping technique for the rapid sampling of rat liver for studies on enzymes in separate cell fractions. Suitability for the study of enzymes regulated by reversible phosphorylation-dephosphorylation. *Biochem J* 220: 733–738, 1984.
9. **Ferrer A, Caelles C, Massot N, and Hegardt FG.** Activation of rat liver cytosolic 3-hydroxy-3-methylglutaryl coenzyme A reductase kinase by adenosine 5′-monophosphate. *Biochem Biophys Res Commun* 132: 497–504, 1985.
10. **Frosig C, Jorgensen SB, Hardie DG, Richter EA, and Wojtaszewski JF.** 5′-AMP-activated protein kinase activity and protein expression are regulated by endurance training in human skeletal muscle. *Am J Physiol Endocrinol Metab* 286: E411–E417, 2004.
11. **Fryer LG, Parbu-Patel A, and Carling D.** The Anti-diabetic drugs rosiglitazone and metformin stimulate AMP-activated protein kinase through distinct signaling pathways. *J Biol Chem* 277: 25226–25232, 2002.
12. **Fujii N, Hayashi T, Hirshman MF, Smith JT, Habinowski SA, Kaijser L, Mu J, Ljungqvist O, Birnbaum MJ, Witters LA, Thorell A, and Goodyear LJ.** Exercise induces isoform-specific increase in 5′ AMP-activated protein kinase activity in human skeletal muscle. *Biochem Biophys Res Commun* 273: 1150–1155, 2000.
13. **Goodman MN and Lowenstein JM.** The purine nucleotide cycle. Studies of ammonia production by skeletal muscle in situ and in perfused preparations. *J Biol Chem* 252: 5054–5060, 1977.
14. **Hardie DG and Carling D.** The AMP-activated protein kinase—fuel gauge of the mammalian cell? *Eur J Biochem* 246: 259–273, 1997.
15. **Hardie DG and Pan DA.** Regulation of fatty acid synthesis and oxidation by the AMP-activated protein kinase. *Biochem Soc Trans* 30: 1064–1070, 2002.
16. **Hawley SA, Boudeau J, Reid JL, Mustard KJ, Udd L, Makela TP, Alessi DR, and Hardie DG.** Complexes between the LKB1 tumor suppressor, STRAD alpha/beta and MO25 alpha/beta are upstream kinases in the AMP-activated protein kinase cascade. *J Biol* 2: 28.1–28.16, 2003.
17. **Hawley SA, Davison M, Woods A, Davies SP, Beri RK, Carling D, and Hardie DG.** Characterization of the AMP-activated protein kinase kinase from rat liver and identification of threonine 172 as the major site at which it phosphorylates AMP-activated protein kinase. *J Biol Chem* 271: 27879–27887, 1996.
18. **Hawley SA, Pan DA, Mustard KJ, Ross L, Bain J, Edelman AM, Frenguelli BG, and Hardie DG.** Calmodulin-dependent protein kinase kinase-beta is an alternative upstream kinase for AMP-activated protein kinase. *Cell Metab* 2: 9–19, 2005.
19. **Hawley SA, Selbert MA, Goldstein EG, Edelman AM, Carling D, and Hardie DG.** 5′ -AMP activates the AMP-activated protein kinase cascade, and Ca2+/calmodulin activates the calmodulin-dependent protein kinase I cascade, via three independent mechanisms. *J Biol Chem* 270: 27186–27191, 1995.
20. **Hayashi T, Hirshman MF, Fujii N, Habinowski SA, Witters LA, and Goodyear LJ.** Metabolic stress and altered glucose transport: activation of AMP-activated protein kinase as a unifying coupling mechanism. *Diabetes* 49: 527–531, 2000.
21. **Hayashi T, Hirshman MF, Kurth EJ, Winder WW, and Goodyear LJ.** Evidence for 5′ AMP-activated protein kinase mediation of the effect of muscle contraction on glucose transport. *Diabetes* 47: 1369–1373, 1998.
22. **Higaki Y, Hirshman MF, Fujii N, and Goodyear LJ.** Nitric oxide increases glucose uptake through a mechanism that is distinct from the insulin and contraction pathways in rat skeletal muscle. *Diabetes* 50: 241–247, 2001.
23. **Hurley RL, Anderson KA, Franzone JM, Kemp BE, Means AR, and Witters LA.** The Ca2+/calmodulin-dependent protein kinase kinases are AMP-activated protein kinase kinases. *J Biol Chem* 280: 29060–29066, 2005.
24. **Hurst D, Taylor EB, Cline TD, Greenwood LJ, Compton CL, Lamb JD, and Winder WW.** AMP-activated protein kinase kinase activity and phosphorylation of AMP-activated protein kinase in contracting muscle of sedentary and endurance-trained rats. *Am J Physiol Endocrinol Metab* 289: E710–E715, 2005.
25. **Hutber CA, Hardie DG, and Winder WW.** Electrical stimulation inactivates muscle acetyl-CoA carboxylase and increases AMP-activated protein kinase. *Am J Physiol Endocrinol Metab* 272: E262–E266, 1997.
26. **Ingebritsen TS, Lee HS, Parker RA, and Gibson DM.** Reversible modulation of the activities of both liver microsomal hydroxymethylglutaryl coenzyme A reductase and its inactivating enzyme. Evidence for regulation by phosphorylation-dephosphorylation. *Biochem Biophys Res Commun* 81: 1268–1277, 1978.
27. **Jorgensen SB, Viollet B, Andreelli F, Frosig C, Birk JB, Schjerling P, Vaulont S, Richter EA, and Wojtaszewski JF.** Knockout of the alpha2 but not alpha1 5′ -AMP-activated protein kinase isoform abolishes 5-aminoimidazole-4-carboxamide-1-beta-4-ribofuranoside but not contraction-induced glucose uptake in skeletal muscle. *J Biol Chem* 279: 1070–1079, 2004.

28. **Kemppainen J, Fujimoto T, Kalliokoski KK, Viljanen T, Nuutila P, and Knuuti J.** Myocardial and skeletal muscle glucose uptake during exercise in humans. *J Physiol* 542: 403–412, 2002.
29. **Langfort J, Viese M, Ploug T, and Dela F.** Time course of GLUT4 and AMPK protein expression in human skeletal muscle during one month of physical training. *Scand J Med Sci Sports* 13: 169–174, 2003.
30. **Lund S, Holman GD, Schmitz O, and Pedersen O.** Contraction stimulates translocation of glucose transporter GLUT4 in skeletal muscle through a mechanism distinct from that of insulin. *Proc Natl Acad Sci USA* 92: 5817–5821, 1995.
31. **McGee SL, Howlett KF, Starkie RL, Cameron-Smith D, Kemp BE, and Hargreaves M.** Exercise increases nuclear AMPK alpha2 in human skeletal muscle. *Diabetes* 52: 926–928, 2003.
32. **Minokoshi Y, Kim YB, Peroni OD, Fryer LG, Muller C, Carling D, and Kahn BB.** Leptin stimulates fatty-acid oxidation by activating AMP-activated protein kinase. *Nature* 415: 339–343, 2002.
33. **Moore F, Weekes J, and Hardie DG.** Evidence that AMP triggers phosphorylation as well as direct allosteric activation of rat liver AMP-activated protein kinase. A sensitive mechanism to protect the cell against ATP depletion. *Eur J Biochem* 199: 691–697, 1991.
34. **Mu J, Brozinick JT Jr, Valladares O, Bucan M, and Birnbaum MJ.** A role for AMP-activated protein kinase in contraction- and hypoxia-regulated glucose transport in skeletal muscle. *Mol Cell* 7: 1085–1094, 2001.
35. **Musi N, Hayashi T, Fujii N, Hirshman MF, Witters LA, and Goodyear LJ.** AMP-activated protein kinase activity and glucose uptake in rat skeletal muscle. *Am J Physiol Endocrinol Metab* 280: E677–E684, 2001.
36. **Nielsen JN, Mustard KJ, Graham DA, Yu H, MacDonald CS, Pilegaard H, Goodyear LJ, Hardie DG, Richter EA, and Wojtaszewski JF.** 5′ -AMP-activated protein kinase activity and subunit expression in exercise-trained human skeletal muscle. *J Appl Physiol* 94: 631–641, 2003.
37. **Park SH, Gammon SR, Knippers JD, Paulsen SR, Rubink DS, and Winder WW.** Phosphorylation-activity relationships of AMPK and acetyl-CoA carboxylase in muscle. *J Appl Physiol* 92: 2475–2482, 2002.
38. **Pold R, Jensen LS, Jessen N, Buhl ES, Schmitz O, Flyvbjerg A, Fujii N, Goodyear LJ, Gotfredsen CF, Brand CL, and Lund S.** Long-term AICAR administration and exercise prevents diabetes in ZDF rats. *Diabetes* 54: 928–934, 2005.
39. **Ponticos M, Lu QL, Morgan JE, Hardie DG, Partridge TA, and Carling D.** Dual regulation of the AMP-activated protein kinase provides a novel mechanism for the control of creatine kinase in skeletal muscle. *EMBO J* 17: 1688–1699, 1998.
40. **Sakamoto K, Goransson O, Hardie DG, and Alessi DR.** Activity of LKB1 and AMPK-related kinases in skeletal muscle: effects of contraction, phenformin, and AICAR. *Am J Physiol Endocrinol Metab* 287: E310–E317, 2004.
41. **Salt I, Celler JW, Hawley SA, Prescott A, Woods A, Carling D, and Hardie DG.** AMP-activated protein kinase: greater AMP dependence, and preferential nuclear localization, of complexes containing the alpha2 isoform. *Biochem J* 334: 177–187, 1998.
42. **Stapleton D, Mitchelhill KI, Gao G, Widmer J, Michell BJ, Teh T, House CM, Fernandez CS, Cox T, Witters LA, and Kemp BE.** Mammalian AMP-activated protein kinase subfamily. *J Biol Chem* 271: 611–614, 1996.
43. **Stein SC, Woods A, Jones NA, Davison MD, and Carling D.** The regulation of AMP-activated protein kinase by phosphorylation. *Biochem J* 345: 437–443, 2000.
44. **Stephens TJ, Chen ZP, Canny BJ, Michell BJ, Kemp BE, and McConell GK.** Progressive increase in human skeletal muscle AMPKalpha2 activity and ACC phosphorylation during exercise. *Am J Physiol Endocrinol Metab* 282: E688–E694, 2002.
45. **Toyoda T, Hayashi T, Miyamoto L, Yonemitsu S, Nakano M, Tanaka S, Ebihara K, Masuzaki H, Hosoda K, Inoue G, Otaka A, Sato K, Fushiki T, and Nakao K.** Possible involvement of the α1-isoform of 5′ -AMP-activated protein kinase in oxidative stress-stimulated glucose transport in skeletal muscle. *Am J Physiol Endocrinol Metab* 287: E166–E173, 2004.
46. **Vavvas D, Apazidis A, Saha AK, Gamble J, Patel A, Kemp BE, Witters LA, and Ruderman NB.** Contraction-induced changes in acetyl-CoA carboxylase and 5′ -AMP-activated kinase in skeletal muscle. *J Biol Chem* 272: 13255–13261, 1997.
47. **Weekes J, Hawley SA, Corton J, Shugar D, and Hardie DG.** Activation of rat liver AMP-activated protein kinase by kinase kinase in a purified, reconstituted system. Effects of AMP and AMP analogues. *Eur J Biochem* 219: 751–757, 1994.
48. **Winder WW, Hardie DG, Mustard KJ, Greenwood LJ, Paxton BE, Park SH, Rubink DS, and Taylor EB.** Long-term regulation of AMP-activated protein kinase and acetyl-CoA carboxylase in skeletal muscle. *Biochem Soc Trans* 31: 182–185, 2003.
49. **Winder WW, Wilson HA, Hardie DG, Rasmussen BB, Hutber CA, Call GB, Clayton RD, Conley LM, Yoon S, and Zhou B.** Phosphorylation of rat muscle acetyl-CoA carboxylase by AMP-activated protein kinase and protein kinase A. *J Appl Physiol* 82: 219–225, 1997.
50. **Wojtaszewski JF, Nielsen P, Hansen BF, Richter EA, and Kiens B.** Isoform-specific and exercise intensity-dependent activation of 5′ -AMP-activated protein kinase in human skeletal muscle. *J Physiol* 528: 221–226, 2000.
51. **Zou MH, Hou XY, Shi CM, Kirkpatick S, Liu F, Goldman MH, and Cohen RA.** Activation of 5′ -AMP-activated kinase is mediated through c-Src and phosphoinositide 3-kinase activity during hypoxia-reoxygenation of bovine aortic endothelial cells. Role of peroxynitrite. *J Biol Chem* 278: 34003–34010, 2003.

0013-7227/06/$15.00/0
Printed in U.S.A.

Endocrinology 147(3):1314–1321

doi: 10.1210/en.2005-1244

Direct Effects of Aldosterone on Cardiomyocytes in the Presence of Normal and Elevated Extracellular Sodium

Megumi Yamamuro, Michihiro Yoshimura, Masafumi Nakayama, Koji Abe, Makoto Shono, Satoru Suzuki, Tomohiro Sakamoto, Yoshihiko Saito, Kazuwa Nakao, Hirofumi Yasue, and Hisao Ogawa

Department of Cardiovascular Medicine (Me.Y., Mi.Y., M.N., K.A., M.S., S.S., T.S., H.O.), Graduate School of Medical Sciences, Kumamoto University, Kumamoto 860-8556, Japan; First Department of Internal Medicine (Y.S.), Nara Medical University, Nara 634-8521, Japan; Department of Medicine and Clinical Science (K.N.), Kyoto University Graduate School of Medicine, Kyoto 606-8501, Japan; and Division of Cardiology (H.Y.), Kumamoto Aging Research Institute, Kumamoto 860-8518, Japan

It is now recognized that aldosterone is potentially cardiotoxic, although its local effects in the heart are not well understood. We examined the effects of aldosterone on cultured neonatal rat cardiomyocytes in the presence of normal and elevated extracellular Na^+ ($[Na^+]_o$). We evaluated the intracellular volume of cardiomyocytes in the presence of normal (141 mEq/liter) and elevated (146 mEq/liter) $[Na^+]_o$ by measuring cell size. Intracellular Na^+ was measured using sodium-binding-benzofuran-isophthalate as a fluorescent sodium indicator, and cardiac hypertrophy was assessed using B-type natriuretic peptide transcription and ^{3}H-leucine incorporation. Cardiomyocytes shrank in the presence of 146 mEq/liter Na^+ due to the increased extracellular osmolarity at early phase. Aldosterone (10^{-7} mol/liter) mitigated the shrinkage by stimulating Na^+ uptake by the cells. This effect of aldosterone was blocked by SM 20220, a Na^+/H^+ exchanger 1 (NHE1) inhibitor, but not by eplerenone, a mineralocorticoid receptor blocker. Seventy-two hours of exposure to aldosterone in the presence of 146 mEq/liter Na^+ led to increases in cardiomyocyte size, ^{3}H-leucine incorporation, and B-type natriuretic peptide and NHE1 transcription that were significantly greater than were seen in the presence of 141 mEq/liter Na^+. All but the last were blocked by either eplerenone or SM 20220; the increase in NHE1 transcription was blocked only by eplerenone. Aldosterone exerts a beneficial effect via NHE1 to block cardiomyocyte shrinkage in the presence of elevated $[Na^+]_o$ at early phase, but long-time exposure to aldosterone in the presence of elevated $[Na^+]_o$ leads to cardiomyocyte hypertrophy via genomic effects mediated by the mineralocorticoid receptor. (*Endocrinology* 147: 1314–1321, 2006)

THE BODY RESPONDS to a salty meal by decreasing the secretion of aldosterone from the adrenal cortex, increasing the secretion of antidiuretic hormone from the posterior pituitary, and activating drinking behavior, thereby stabilizing levels of circulating Na^+ (1, 2). However, if one's diet is continuously high in Na^+ or if a large amount of Na^+ is acutely taken in, the circulating Na^+ level will tend to rise. When that happens, somatic cells are subject to fluid loss due to the increase in the extracellular osmolarity, which causes them to shrink. Oxidative stress is also increased, and a life-threatening crisis can occur in severe cases (3, 4). But despite its vital importance, the regulatory system that strictly governs the levels of circulating Na^+ is not well understood.

Aldosterone has traditionally been seen as a key regulator of fluid and electrolyte balance, acting via the mineralocorticoid receptor (MR) in the epithelium of the kidney (distal nephron), colon, and salivary glands (5). However, we recently showed that aldosterone is also synthesized in the hearts of patients with heart failure or hypertension (6–8), and that in neonatal rat cardiomyocytes it induces expression of angiotensin-converting enzyme, creating a vicious circular cascade involving the renin-angiotensin-aldosterone-system (9). In addition, others have shown that aldosterone induces vascular inflammation and apoptosis within the cardiovascular system (10, 11). The molecular mechanisms by which aldosterone exerts its local effects are not fully characterized, however.

The Na^+/H^+ exchanger 1 (NHE1) is a ubiquitously expressed housekeeping transporter that catalyzes the electroneutral countertransport of extracellular Na^+ and intracellular protons (12, 13). In addition to mediating the transcellular absorption of Na^+, NHE1 plays a major role in the regulation of intracellular pH, cell volume and, possibly, cell proliferation (13). Aldosterone regulates Na^+ homeostasis and, consequently, extracellular volume in large part by controlling NHE1 activity in the kidney (12–14). There are also reports that aldosterone up-regulates NHE1 activity by both genomic or nongenomic means (15, 16); that NHE1 serves as a critical downstream regulator contributing to cardiac remodeling in response to various hypertrophic factors (16, 17); and that inhibition of NHE1 suppresses progression of cardiac hypertrophy (18).

With that as background, we hypothesized that, in the face of an acute increase in the extracellular Na^+ concentration ($[Na^+]_o$), aldosterone would act nongenomically on NHE1 to promote cellular Na^+ uptake and fluid retention to attenuate cell shrinkage. If those conditions persisted, however, aldo-

First Published Online December 22, 2005

Abbreviations: BNP, B-type natriuretic peptide; ENaC, epithelial Na^+ channel; MR, mineralocorticoid receptor; Na^+/K^+ ATPase, Na^+/K^+ adenosine triphosphatase; NHE1, Na^+/H^+ exchanger 1; SBFI, sodium-binding-benzofuran-isophthalate; SBFI-AM, SBFI-acetoxymethyl ester.

Endocrinology is published monthly by The Endocrine Society (http://www.endo-society.org), the foremost professional society serving the endocrine community.

sterone would act genomically, causing cardiomyocyte hypertrophy by way of NHE1. To test this hypothesis, we investigated the direct actions of aldosterone—*i.e.* those independent of hemodynamic overload—in cultured neonatal rat cardiomyocytes.

Materials and Methods

In this *in vitro* study, $[Na^+]_o$ was either 141 mEq/liter or 146 mEq/liter, which is within the physiological range. Cellular fluid changes were evaluated by measuring cell size (19) and changes in the intracellular Na^+ concentration ($[Na^+]_i$) were measured using sodium-binding benzofuran isophthalate (SBFI), a fluorescent Na^+ indicator (20). To examine NHE1 activity, intracellular H^+ concentration ($[H^+]_i$) was measured using LysoSensor Green DND-153 (21). Cardiac hypertrophy was assessed using ^{3}H-leucine incorporation (22) and B-type natriuretic peptide (BNP) gene expression (9, 19, 23), two sensitive makers of cardiac hypertrophy, as indices. In addition, we also tested the effects of eplerenone, a specific MR blocker (24), and SM 20220, a NHE1 inhibitor (25), on the genomic and nongenomic actions of aldosterone.

Agents used

Aldosterone was purchased from Steraloid Co. (Wilton, NH). SBFI-acetoxymethyl ester (SBFI-AM) was purchased from Sigma Chemical Co. (St. Louis, MO) (20). LysoSensor Green DND-153 as a pH indicator was purchased from Molecular Probes (Eugene, OR) (21). Eplerenone was provided by Pfizer Co., Ltd. (New York, NY) (24). SM 20220, which is a specific inhibitor of NHE1 in cultured neurons and glial cells with an IC_{50} of 5 and 20 nM, respectively, was provided by Sumitomo Pharmaceuticals Co., Ltd., Research Division (Osaka, Japan) (25, 26).

Preparation of cardiomyocytes

All animal procedures conformed to the National Institutes of Health Guide for the Care and Use of Laboratory Animals and were approved by the Animal Research Committee at Kumamoto University. Cardiomyocytes were obtained from 1- to 2-d-old Wistar rats. Ventricular cells were dispersed in a balanced Na^+ solution containing 0.04% collagenase II (Sigma) and 0.06% pancreatin (Sigma) (9, 19, 22, 23). The cardiomyocytes were isolated on a discontinuous Percoll gradient using 40.5% and 58.5% Percoll (Sigma) prepared in balanced Na^+ solution. Ventricular cells were initially suspended in the 58.5% Percoll layer (19, 22, 23). After centrifugation at 3000 rpm for 30 min at 15 C, the cardiomyocytes had migrated to the interface between the layers.

Cell culture

Purified cardiomyocytes were plated at a density of 3.0×10^4 cells/cm^2 in six-well plates (2.9×10^5 cells/well) in DMEM (GIBCO, Carlsbad, CA) supplemented with 10% fetal bovine serum (Moregate Bio Tech, Bulimba, Australia) and antibiotics (100 U/ml penicillin G and 100 μg/ml streptomycin; GIBCO). The cells were allowed to attach for 30 h, after which the medium was replaced with serum-free DMEM, and the cells were incubated for an additional 12 h. After this preconditioning period, the cells were incubated in serum-free DMEM containing 1 mg/ml BSA (Sigma) with the indicated test substances (9, 19, 22, 23). Medium containing 146 mEq/liter Na^+ was made by simply adding NaCl (Wako, Osaka, Japan) to the normal 141 mEq/liter Na^+ medium (27). pH was 7.3 ± 0.2 in both media.

Measurement of cell size

Surface areas of cardiomyocytes were measured using Lumina Vision (Mitani Co., Fukui, Japan). Cardiomyocytes in the culture wells were chosen at random for measuring cell sizes from five to eight preparations and two different people blindly measured cell sizes.

^{3}H-leucine incorporation

Cardiomyocytes were plated at 3.0×10^4 cells/cm^2 in 96-well dishes and treated as described above. ^{3}H-leucine (3 μCi/ml, 2.15×10^{-8} mol/liter; PerkinElmer, Yokohama, Japan) was then added to each well just after the last treatment, as previously described (22). After incubating 72 h, the cells were harvested using an Omnifilter-96 Harvester (PerkinElmer) (28), and ^{3}H-leucine incorporation was measured using a MicroBeta TriLux (PerkinElmer) (28).

Quantitative real-time RT-PCR

For real-time RT-PCR, total RNA was extracted from cardiomyocytes cultured in six-well plates using an RNeasy Mini Kit (QIAGEN, Bulimba, Germany) (9, 23) and treated with deoxyribonuclease I (QIAGEN) to eliminate any contaminating genomic DNA (9, 23). The oligonucleotide primers and TaqMan probes used to analyze expression of rat BNP mRNA were designed from GenBank databases (M25297) using Primer Express version 1.0 (Applied Biosystems, Foster City, CA) as previously described (9, 23). The forward primer was 5′-181-CAG AAG CTG CTG GAG CTG ATA AG-203-3′; the reverse primer was 5′-258-TGT AGG GCC TTG GTC CTT TG-239-3′; and the TaqMan probe was 5′-207-AAA GTC AGA GGA AAT GGC TCA GAG ACA GCT C-237-3′. Primers and the TaqMan probe set for rat NHE1 (No. 185248084) were purchased from Assays-on-Demand Gene Expression Products (Applied Biosystems), and those for rat glyceraldehyde-3-phosphate dehydrogenase were from PerkinElmer Applied Biosystems. Two-step real time RT-PCR was carried out using TaqMan Reverse Transcription Reagents (Applied Biosystems) and a TaqMan Universal Master Mix kit (Applied Biosystems) (29) with an ABI Prism 7900 sequence detection system (Applied Biosystems) (29).

Measurement of BNP and NHE1 protein levels

We measured BNP levels in these culture mediums after 72 h using a BNP ELISA Kit (Peninsula Laboratories Inc., San Carlos, CA). NHE1 protein levels were measured by Western blotting using a polyclonal antibody (Santa Cruz Biotechnology, Santa Cruz, CA) after 72 h culture as described (16).

Measurement of intracellular Na^+

After incubating cardiomyocytes for 2 h in medium containing 141 or 146 mEq/liter Na^+, $[Na^+]_i$ was determined as previously described (20). Briefly, cardiomyocytes grown on glass-bottomed dishes were incubated with 10 μmol/liter SBFI-AM for 90 min at room temperature in presence of the nonionic surfactant Pluronic F-127 (0.05% wt/vol; Sigma). After washing out the external dye, we allowed the intracellular SBFI-AM to be deesterified to active SBFI for 20 min before proceeding with $[Na^+]_i$ measurements. The cells were incubated in DMEM containing 141 and 146 mEq/liter Na^+, and $[Na^+]_i$ levels at a single cell were measured as a function of SBFI fluorescence using an Ion Optix dual-wavelength ratiometric photon counting system (11). The cells were pretreated with SM 20220 or eplerenone just before this measuring. After measuring for 60 sec, 10^{-7} mol/liter aldosterone was added to the medium.

Measurement of intracellular H^+

After incubating cardiomyocytes for 2 h in a medium containing 141 or 146 mEq/liter Na^+, intracellular H^+ levels ($[H^+]_i$) were examined (21). Cardiomyocytes grown on glass-bottomed dishes were incubated with 1 μmol/liter LysoSensor Green DND-153 for 30 min. After washing out the external dye, the cells were incubated in DMEM containing 141 and 146 mEq/liter Na^+, and $[H^+]_i$ levels in a single cell with 10^{-7} mol/liter aldosterone were measured using LysoSensor Green DND-153 fluorescence with Lumina Vision (Mitani Co., Fukui, Japan). The cells were pretreated with SM 20220 or eplerenone just before this measurement.

Statistical analysis

Data are expressed as means ± SEM. Statistical analysis was performed using one-way ANOVA followed by multiple comparisons using Fisher's protected least-significant difference and unpaired Student's *t* tests, as appropriate. Values of $P < 0.05$ were considered significant.

Results

In the present study, we evaluate the actions of aldosterone in time course divided into early phase (0–6 h) and late phase (72 h).

Effect of aldosterone on cardiomyocyte size in the presence of normal and elevated $[Na^+]_o$ at early phase

Figure 1A shows the morphology of neonatal rat cardiomyocytes after 2 h in the presence of normal (141 mEq/liter) or elevated (146 mEq/liter) $[Na^+]_o$ with and without 10^{-7} mol/liter aldosterone. There was no change in the size of the cells in the presence of 141 mEq/liter Na^+ with or without aldosterone. In the presence of 146 mEq/liter Na^+ without aldosterone, however, the cells became substantially smaller, and this shrinkage was blocked by the addition of aldosterone.

Figure 1B shows the time-dependent changes in the size of cardiomyocytes over a period of 24 h. In the absence of aldosterone, the cells shrank significantly in the presence of 146 mEq/liter Na^+ over the course of 6 h ($P < 0.0001$; *vs.* 141 mEq/liter Na^+ without aldosterone at 1, 2, 3, and 6 h); again, this shrinkage was blocked by addition of 10^{-7} mol/liter aldosterone. The ability of aldosterone to block cell shrinkage in the presence of elevated $[Na^+]_o$ apparently reflects its ability to stimulate Na^+ uptake by the cells and thus increase $[Na^+]_i$. Figure 1C showed the effects of eplerenone and SM 20220 on the cell sizes of cardiomyocytes with 10^{-7} mol/liter aldosterone in the presence of 146 mEq/liter Na^+ at 2 h. SM 20220, but not eplerenone, blocked cell recovery induced by aldosterone in the presence of 146 mEq/liter Na^+.

Effect of aldosterone on the level of intracellular Na^+ and intracellular H^+ in the presence of normal and elevated $[Na^+]_o$ at early phase

In Fig. 2, 10^{-7} mol/liter aldosterone did not elevate intracellular sodium concentrations in SBFI-loaded cardiomyocytes with 141 mEq/liter Na^+ (Fig. 2A). There was an in-

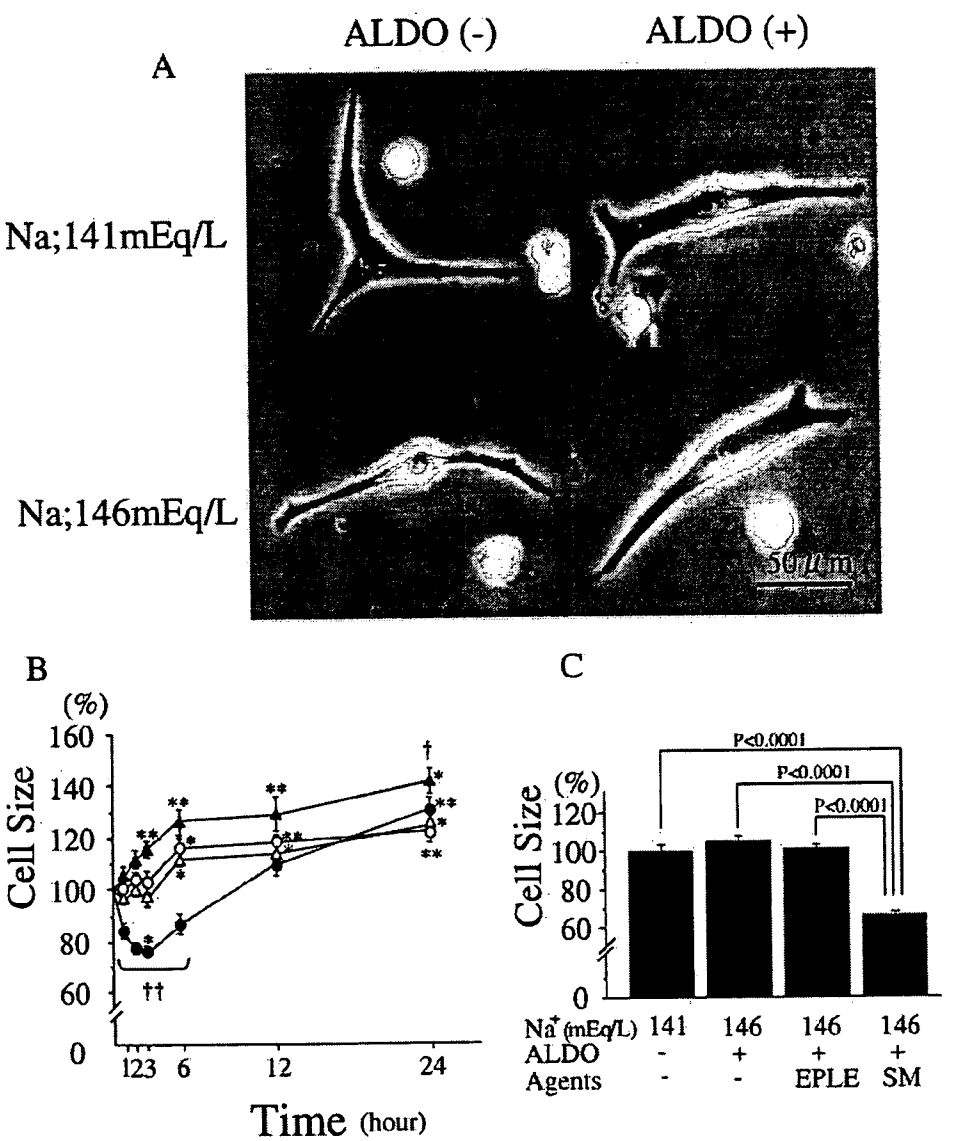

FIG. 1. A, Photomicrographs showing cardiomyocytes after 2 h in the presence of 141 mEq/liter or 146 mEq/liter Na^+ with (+) or without (−) 10^{-7} mol/liter aldosterone (ALDO). B, Time-dependent changes in the sizes of cardiomyocytes during incubation in the presence of 141 mEq/liter or 146 mEq/liter Na^+ with or without 10^{-7} mol/liter aldosterone. *Open circle*, Without 10^{-7} mol/liter aldosterone in the presence of 141 mEq/liter Na^+; *closed circle*, without 10^{-7} mol/liter aldosterone in the presence of 146 mEq/liter Na^+; *open triangle*, with 10^{-7} mol/liter aldosterone in the presence of 141 mEq/liter Na^+; *closed triangle*, with 10^{-7} mol/liter aldosterone in the presence of 146 mEq/liter Na^+. *, $P < 0.01$; **, $P < 0.0001$ *vs.* 0 h; †, $P < 0.01$; ††, $P < 0.0001$ *vs.* 141 mEq/liter Na^+ without aldosterone; n = 20. C, Sizes of cardiomyocytes incubated for 2 h in the presence of 146 mEq/liter Na^+ with 10^{-7} mol/liter aldosterone (ALDO) alone or in combination with 10^{-5} mol/liter eplerenone (EPLE) or 10^{-7} mol/liter SM 20220 (SM); n = 20.

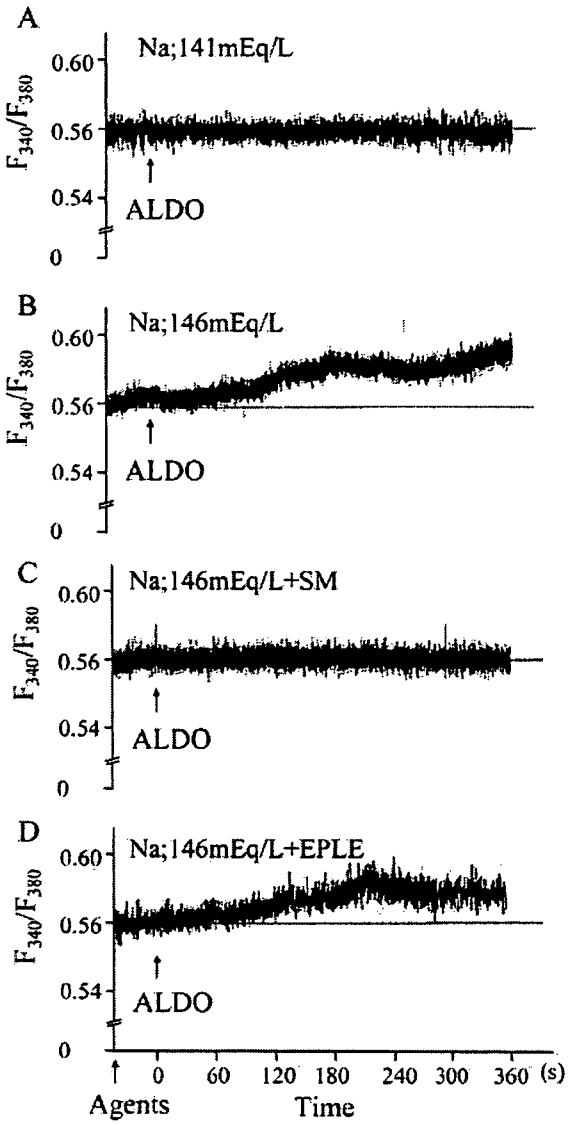

FIG. 2. Fluorescence ratios indicating the time-dependent changes in $[Na^+]_i$ at $[Na^+]_o$ = 141 or 146 mEq/liter. The *arrow* indicates addition of 10^{-7} mol/liter aldosterone (ALDO). A, In the presence of 141 mEq/liter Na^+; B, in the presence of 146 mEq/liter Na^+; C, with 10^{-7} mol/liter SM 20220 (SM) in the presence of 146 mEq/liter Na^+; D, with 10^{-5} mol/liter eplerenone (EPLE) in the presence of 146 mEq/liter Na^+.

crease in $[Na^+]_i$ after adding 10^{-7} mol/liter aldosterone to cardiomyocytes in the presence of 141 and 146 mEq/liter Na^+ (Fig. 2B). It appears that the aldosterone-induced Na^+ uptake was mediated by the NHE1, as the effect was significantly inhibited by the NHE1 antagonist SM 20220 (10^{-7} mol/liter) (Fig. 2C). In contrast, the MR antagonist eplerenone (10^{-5} mol/liter) had no effect (Fig. 2D).

In Fig. 3, we measured the level of intracellular H^+ ($[H^+]_i$) in the cardiomyocytes using LysoSensor Green DND-153 with 10^{-7} mol/liter aldosterone for examination of the activity of NHE1. Levels of $[H^+]_i$ in the cardiomyocytes with 10^{-7} mol/liter aldosterone in the presence of 146 mEq/liter Na^+ were significantly lower than those in the presence of 141 mEq/liter Na^+. SM 20220 blocked aldosterone-induced

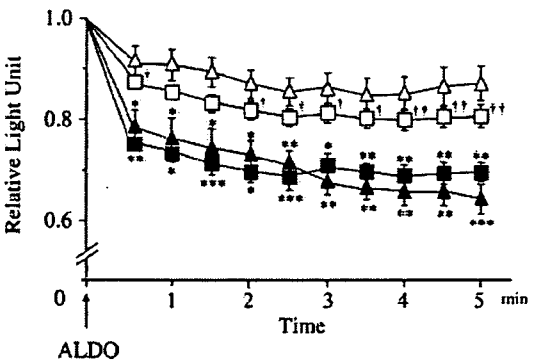

FIG. 3. Fluorescence ratios with 10^{-7} mol/liter aldosterone (ALDO) indicating the time-dependent changes in $[H^+]_i$ at $[Na^+]_o$ = 141 or 146 mEq/liter. *Open triangle*, In the presence of 141 mEq/liter Na^+, *closed triangle*, in the presence of 146 mEq/liter Na^+, *open square*, with 10^{-7} mol/liter SM 20220 in the presence of 146 mEq/liter Na^+; *closed square*, with 10^{-5} mol/liter eplerenone in the presence of 146 mEq/liter Na^+. *, $P < 0.05$; **, $P < 0.005$; ***, $P < 0.0005$ *vs.* fluorescence ratios with 10^{-7} mol/liter aldosterone in the presence of 141 mEq/liter Na^+ at each time; †, $P < 0.05$; ††, $P < 0.005$ *vs.* fluorescence ratios with 10^{-7} mol/liter aldosterone in the presence of 146 mEq/liter Na^+ at each time; n = 8.

H^+ discharge, but eplerenone did not block aldosterone-induced H^+ discharge in the presence of 146 mEq/liter Na^+.

Effect of aldosterone on cardiomyocytes size in the presence of normal and elevated $[Na^+]_o$ at late phase

Seventy-two hours of exposure to 10^{-7} mol/liter aldosterone significantly increased cardiomyocyte size in the presence of both 141 mEq/liter and 146 mEq/liter Na^+ ($P < 0.005$, $P < 0.0005$, respectively), although the increase was significantly greater the presence of the latter ($P < 0.0005$ *vs.* normal Na^+) (Figs. 4A and 5A). The effect of aldosterone on cell size was significantly attenuated by either eplerenone or SM 20220 in the presence of 146 mEq/liter $[Na^+]_o$ (both $P < 0.0005$) (Figs. 4B and 5A). In the absence of aldosterone, neither eplerenone nor SM 20220 affected the cell size in the presence of 141 mEq/liter Na^+ at 72 h. In Figs. 1A and 4, they were different cells before and after aldosterone stimulation.

Effect of aldosterone on ^{3}H-leucine incorporation by cardiomyocytes at late phase

Indicative of induction of cell hypertrophy, 10^{-7} mol/liter aldosterone significantly increased ^{3}H-leucine incorporation by cardiomyocytes in the presence of either 141 mEq/liter or 146 mEq/liter Na^+ at late phase ($P < 0.05$, $P < 0.05$, respectively) and, as with cell size, the effect was more pronounced in the presence of the latter (Fig. 5B). This effect in the presence of 146 mEq/liter Na^+ was significantly attenuated by inhibiting NHE1 using SM 20220 ($P < 0.0005$). In the absence of aldosterone, neither eplerenone nor SM 20220 affected ^{3}H-leucine incorporation in the presence of 141 mEq/liter Na^+ at 72 h.

Effect of aldosterone on BNP gene expression and BNP expression by cardiomyocytes at late phase

We found that long-time exposure to 10^{-7} mol/liter aldosterone in the presence of 146 mEq/liter Na^+ induced a significant increase in BNP gene expression by cardiomyo-

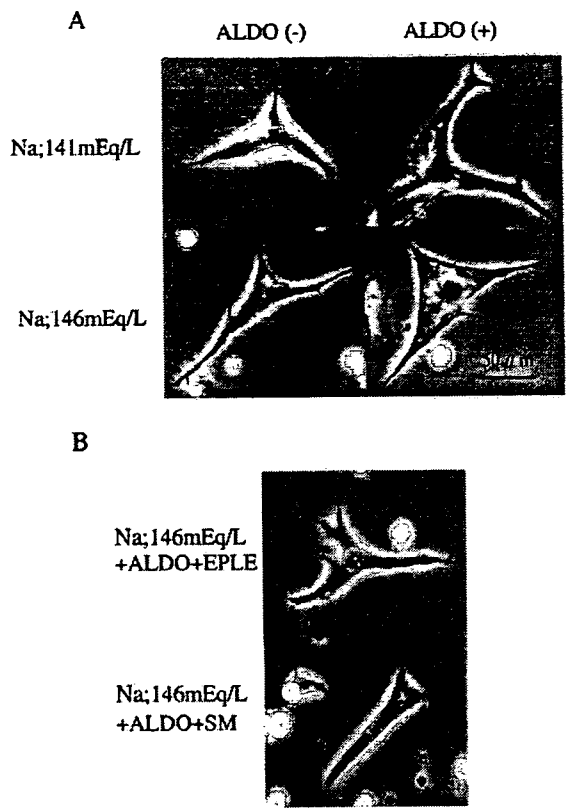

FIG. 4. A, Photomicrographs showing cardiomyocytes after 72 h in the presence of 141 mEq/liter or 146 mEq/liter Na^+ with (+) or without (−) 10^{-7} mol/liter aldosterone (ALDO). B, Photomicrographs showing cardiomyocytes after 72 h in the presence of 146 mEq/liter Na^+ with 10^{-7} mol/liter aldosterone (ALDO) alone or in combination with 10^{-5} mol/liter eplerenone (EPLE) or 10^{-7} mol/liter SM 20220 (SM).

cytes ($P < 0.0005$) that was accompanied by a substantial increase in cell size (Fig. 5C). Moreover, the effect of aldosterone on BNP gene expression was significantly greater in the presence of 146 mEq/liter Na^+ than in the presence of 141 mEq/liter Na^+ ($P < 0.05$). Both the BNP gene expression and the hypertrophy were attenuated by either eplerenone or SM 20220 ($P < 0.005$, $P < 0.0005$, respectively, for BNP gene expression). Eplerenone and SM 20220, without aldosterone, did not affect BNP gene expression levels in the presence of 141 mEq/liter Na^+ at 72 h. SM 20220 or eplerenone with 10^{-7} mol/liter aldosterone did not inhibit the effect of aldosterone by these parameters in the presence of 141 mEq/liter Na^+ at 72 h.

In the supplemental figure published on The Endocrine Society's Journals Online web site at http://endo.endojournals.org, 10^{-7} mol/liter aldosterone significantly increased BNP levels in cardiomyocytes in the presence of either 141 mEq/liter or 146 mEq/liter Na^+ at the late phase ($P < 0.05$, $P < 0.05$, respectively) and, as with BNP gene expression, the effect was more pronounced in the presence of the latter. This effect in the presence of 146 mEq/liter Na^+ was significantly attenuated by inhibiting NHE1 using SM 20220 ($P < 0.05$). In the absence of aldosterone, eplerenone and SM 20220 did not affect BNP levels in the presence of 141 mEq/liter Na^+ at 72 h.

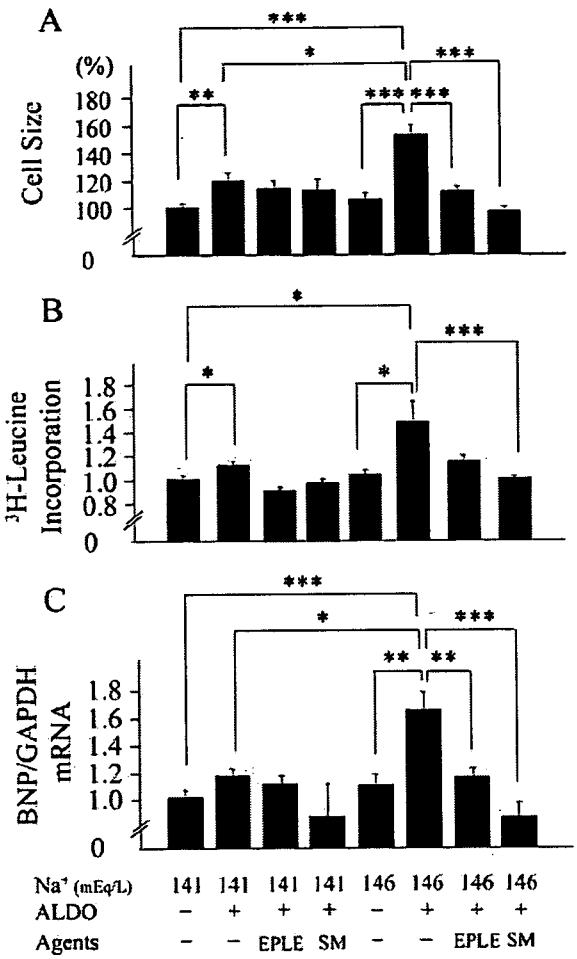

FIG. 5. Effects of aldosterone and $[Na^+]_o$ on cell size (A), ^{3}H-leucine incorporation (B), and BNP gene expression (C) at late phase. Cardiomyocytes were incubated for 72 h in the presence 141 mEq/liter or 146 mEq/liter Na^+ with or without 10^{-7} mol/liter aldosterone (ALDO) alone or in combination with 10^{-5} mol/liter eplerenone (EPLE) or 10^{-7} mol/liter SM 20220 (SM). *, $P < 0.05$; **, $P < 0.005$; ***, $P < 0.0005$; n = 10–20. GAPDH, Glyceraldehyde-3-phosphate dehydrogenase.

Effects of aldosterone on NHE1 gene and protein expression by cardiomyocytes at late phase

NHE1 gene expression was also significantly increased by 10^{-7} mol/liter aldosterone ($P < 0.05$) in the presence of Na^+141 and 146 mEq/liter (Fig. 6A). Aldosterone also increased NHE1 protein levels in the presence of Na^+ 141 and 146 mEq/liter (Fig. 6B). The effect of aldosterone on NHE1 gene expression was significantly attenuated by eplerenone ($P < 0.05$); in contrast, SM 20220 had no effect (Fig. 6A).

Discussion

We found that acute exposure to elevated $[Na^+]_o$ caused cardiomyocytes to rapidly shrink as a result of fluid loss to the outside driven by the increase in extracellular osmolarity. Aldosterone strongly suppressed this loss of fluid by inducing Na^+ uptake, as indicated by the observed increase in SBFI fluorescence, which diminished the osmotic pressure gradient across the cell membrane. We believe these findings show that aldosterone exerts a protective effect against cardiomy-

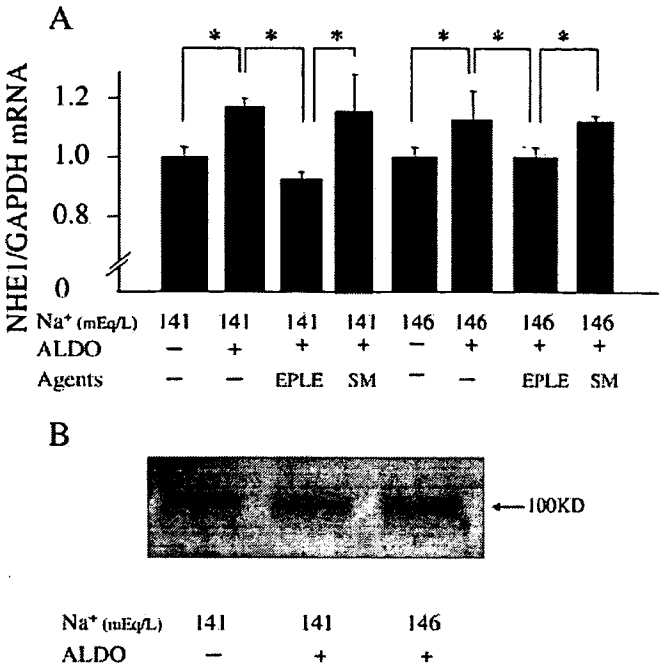

FIG. 6. A, Effect of aldosterone on NHE1 gene expression in cardiomyocytes incubated for 72 h in the presence of 141 or 146 mEq/liter Na^+ with or without 10^{-7} mol/liter aldosterone (ALDO) alone or in combination with 10^{-6} mol/liter eplerenone (EPLE) or 10^{-7} mol/liter SM 20220 (SM). *, $P < 0.05$, n = 10. B, Western blots of NHE1 with or without 10^{-7} mol/liter aldosterone (ALDO) in the presence of 141 or 146 mEq/liter Na^+. GAPDH, Glyceraldehyde-3-phosphate dehydrogenase

ocyte dehydration in the presence of elevated $[Na^+]_o$ at early phase. It appears that this effect is mediated by the NHE1 because it was blocked by the NHE1 antagonist SM 20220. At early phase, we found no evidence that aldosterone acts acutely via the MR, as indicated by eplerenone's lack of effect, or that it acutely induces cellular hypertrophy, as indicated by the absence of up-regulated BNP transcription or ^{3}H-leucine incorporation (data not shown). These findings also suggest that aldosterone may contribute to the rapid regulation and maintenance of circulating Na^+ levels by regulating the movement of Na^+ into cardiomyocytes like principal cells of the kidney distal tubules (30). It has been reported that the nongenomic effects of aldosterone on NHE were blocked by eplerenone in mesenteric resistance vessels (31). We cannot positively deny the effects of aldosterone on NHE1 via the classical MR in cardiomyocytes (31, 32).

In one recent study, aldosterone was shown to induce Na^+ influx into human umbilical vein endothelial cells, leading to cell swelling, even when the Na^+ concentration in the culture medium was unchanged (33). It was suggested that this effect was mediated via the epithelial Na^+ channel (ENaC). At one time, ENaCs were thought to exist only in the kidney; that was until the ENaC δ-subunit was identified in human heart (34). The function and significance of the ENaC in heart is not yet known, but it is possible that, along with NHE1, it contributes to mediating the acute effects of aldosterone in response to a rise in $[Na^+]_o$.

Na^+/K^+ adenosine triphosphatase (Na^+/K^+ ATPase), which mediates the active transport of Na^+ out and K^+ into the cells, is present in cardiomyocytes (35). It is notable that Na^+/K^+ ATPase has been reported to be reversely suppressed by aldosterone in the myocardium (36). Therefore, the inhibitory action of aldosterone on Na^+/K^+ ATPase in the myocardium would not conflict with the possible effect of aldosterone on the intracellular influx of sodium by NHE1 because both actions take sodium into cells in the myocardium.

Secretion of aldosterone from the adrenal gland is diminished by a high Na^+ diet, reducing circulating levels of the hormone (2). On the other hand, it was recently reported that, in rats, the concentration of aldosterone in cardiac and vascular tissues are increased by high Na^+ intake (37). In view of our present findings, we suggest that cell shrinkage caused by the increase in extracellular osmolarity associated with high Na^+ intake would stimulate local synthesis of aldosterone, which in turn stimulates uptake of extracellular Na^+ and water into the cells, thereby stabilizing the electrolyte and fluid balance across the cell membrane. Naturally, we understand that there are many reports disputing the theory about cardiac aldosterone synthesis (38, 39). It is still unclear, however, which of sodium, potassium, chloride, angiotensin II, ACTH, or others is actually the key regulator for cardiac aldosterone synthesis *in vivo* (40, 41). There are many issues that we should study in the future.

In sharp contrast to the effects of aldosterone at early phase, we found that long-time aldosterone exposure induces cardiomyocyte hypertrophy, as indicated by increased cell size, increased incorporation of ^{3}H-leucine, and increased BNP transcription. That these effects could be suppressed by either eplerenone or SM 20220 means that the effects of aldosterone are mediated via both the MR and NHE1 at late phase. In addition, we also found that aldosterone induces NHE1 gene expression via the MR (eplerenone sensitive) at late phase, which is consistent with earlier reports (15, 16).

The effects of aldosterone at late phase observed in the present study are in agreement with those of Karmazyn *et al.* (16) and complement them by adding the observation that aldosterone-induced myocardial hypertrophy is dependent on $[Na^+]_o$ as well as on the NHE1 activity. Elevation of $[Na^+]_i$ via NHE1 likely leads to Ca^{2+} overload via the Na^+/Ca^{2+} exchanger, which would in turn stimulate hypertrophic signaling (42). Also, it is possible that the increase in cell pH directly resulting from NHE1 activation might be the signal for the induction of the hypertrophic response. Furthermore, inflammatory cytokines may be involved in this system of aldosterone-induced myocardial hypertrophy depending on the $[Na^+]_o$ level. In any event, eplerenone would be useful for treating and/or preventing myocardial hypertrophy. The results of both the RALES trial and the EPHESUS trial support this idea for the MR antagonist (43, 44). Also, as suggested by Young and Funder (45), the NHE1 antagonist might also be good for reducing cardiac fibrosis, although this agent has not been used in a clinical stage yet.

We used aldosterone at a concentration of 10^{-7} mol/liter, which is a close approximation to the circulating levels seen *in vivo*, particularly under hyperaldosteronemic conditions. This actually may be somewhat conservative, however, because aldosterone concentrations are reportedly an order of

magnitude higher in cardiac tissues than in the peripheral circulation (40).

The effect of aldosterone in the heart should be discussed because cardiomyocyte MR is normally occupied by endogenous glucocorticoid in physiological status because 11β-hydroxysteroid dehydrogenase type 2 is not normally expressed in the cardiomyocytes and there are high levels of circulating cortisol (46); however, in pathophysiological states, such as hypertension, heart failure, or neonatal stage, it has been hypothesized that mineralocorticoids can access cardiac MR and thereby produce cardiac damage (46).

We previously reported that aldosterone synthesis is activated in both the adrenal gland and hearts of patients with heart failure or hypertension (6–8). Moreover, as mentioned above, aldosterone levels are higher in the myocardium than in the circulation (40). Taken together, these findings suggest that a continuous intake of excess salt stimulates cardiac hypertrophy together with local production of aldosterone in the heart, irrespective of circulating aldosterone levels. Consistent with that idea, we observed that long-time elevated $[Na^+]_o$ induced a small increase in cardiac hypertrophy even in the absence of added aldosterone. This may be explained by the endogenous production of aldosterone by the cells. We have to regardless the fact that there are many reports disputing the theory about cardiac aldosterone synthesis (38, 39) and also that the detrimental effects of aldosterone on the heart may be due to adrenal derived aldosterone (47).

From a clinical viewpoint, the results of the present study highlight the benefit of reducing salt in the diet and are consistent with earlier reports emphasizing the importance maintaining a low-salt diet to prevent cardiac hypertrophy and subsequent heart failure (27). In that regard, our findings indicate that by maintaining a low-salt diet and thus reducing local cardiovascular levels of aldosterone, one mitigates the chronic effects of this potent mediator of cardiac hypertrophy. Observational studies of the Yanomamo Indians, a no-salt culture, reinforce this view (48, 49).

In conclusion, aldosterone acutely induces Na^+ uptake via NHE1 in the presence of elevated $[Na^+]_o$. This rapid, nongenomic protective effect against cellular fluid loss is a positive and physiological attribute. In the face of elevated $[Na^+]_o$, however, long-time exposure to aldosterone induces pathological genomic effects via MR that lead to cardiomyocyte hypertrophy. The MR antagonist eplerenone could thus be useful for suppressing cardiac hypertrophy, without affecting the beneficial effects of aldosterone at early phase.

Acknowledgments

Received September 30, 2005. Accepted December 9, 2005.

Address all correspondence and requests for reprints to: Michihiro Yoshimura, Department of Cardiovascular Medicine, Graduate School of Medical Sciences, Kumamoto University, 1-1-1 Honjo, Kumamoto 860-8556, Japan. E-mail: bnp@kumamoto-u.ac.jp.

This study was supported in part by grants-in-aid from the Ministry of Education, Culture, Sports, Science, and Technology, Tokyo [B (2)-15390248 and B (2)-15390249], the Ministry of Health, Labor and Welfare, Tokyo [14C-4, 14A-1, 17A-1 and 17C-2], the Smoking Research Foundation, Tokyo and the Takeda Science Foundation (Tokyo, Japan).

References

1. Rodrigues J, Castro M, Elias L, Valença MM, McCann SM 2004 Neuroendocrine control of body fluid metabolism. Physiol Rev 84:169–208
2. Ye P, Kenyon CJ, Mackenzie SM, Seckel JR, Fraser R, Connell JMC, Davies E 2003 Regulation of aldosterone synthase gene expression in the rat adrenal gland and central nervous system by sodium and angiotensin II. Endocrinology 144:3321–3328
3. Kültz D, Chakravarty D 2001 Hyperosmolality in the form of elevated NaCl but not urea causes DNA damage in murine kidney cells. Proc Natl Acad Sci USA 98:1999–2004
4. Dmitrieva NI, Cai Q, Burg MB 2004 Cells adapted to high NaCl have many DNA breaks and impaired DNA repair both in cell culture and in vivo. Proc Natl Acad Sci USA 101:2317–2322
5. Garty H, Palmer LG 1997 Epithelial sodium channels: function, structure, and regulation. Physiol Rev 77:359–388
6. Mizuno Y, Yoshimura M, Yasue H, Sakamoto T, Ogawa H, Kugiyama K, Harada E, Nakayama M, Nakamura S, Ito T, Shimasaki Y, Saito Y, Nakao K 2001 Aldosterone production is activated in failing ventricle in humans. Circulation 103:72–77
7. Yamamoto N, Yasue H, Mizuno Y, Yoshimura M, Fujii H, Nakayama M, Harada E, Nakamura S, Ito T, Ogawa H 2002 Aldosterone is produced from the ventricles of patients with essential hypertension. Hypertension 39:958–962
8. Yoshimura M, Nakamura S, Ito T, Nakayama M, Harada E, Mizuno Y, Sakamoto T, Yamamuro M, Saito Y, Nakao K, Yasue H, Ogawa H 2002 Expression of aldosterone synthase gene in failing human heart: quantitative analysis using modified real-time polymerase chain reaction. J Clin Endocrinol Metab 87:3936–3940
9. Harada E, Yoshimura M, Yasue H, Nakagawa O, Nakagawa M, Harada M, Mizuno Y, Nakayama M, Shimasaki Y, Ito T, Nakamura S, Kuwahara K, Saito Y, Nakao K, Ogawa H 2001 Aldosterone induces angiotensin-converting-enzyme gene expression in cultured neonatal rat cardiocytes. Circulation 104:137–139
10. Rocha R, Stier Jr CT 2001 Pathophysiological effects of aldosterone in cardiovascular tissues. Trends Endocrinol Metab 12:308–314
11. Mano A, Tatsumi T, Shiraishi J, Keira N, Nomura T, Takeda M, Nishikawa S, Yamanaka S, Matoba S, Kobara M, Tanaka H, Shirayama T, Takamatsu T, Nozawa Y, Matsubara H 2004 Aldosterone directly induces myocyte apoptosis through calcineurin-dependent pathways. Circulation 110:317–323
12. Orlowski J, Kandasamy RA, Shull GE 1992 Molecular cloning of putative members of the Na^+/H^+ exchanger gene family. J Biol Chem 267:9331–9339
13. Wakabayashi S, Shigekawa M, Pouyssegur J 1997 Molecular physiology of vertebrate Na^+/H^+ exchangers. Physiol Rev 77:51–74
14. Karmazyn M, Gan XT, Humphreys RA, Yoshida H, Kusumoto K 1999 The myocardial Na^+/H^+ exchange: structure, regulation, and its role in heart disease. Circ Res 85:777–786
15. Ebata S, Muto S, Okada K, Nemoto J, Amemiya M, Saito T, Asano Y 1999 Aldosterone activates Na^+/H^+ exchange in vascular smooth muscle cells by nongenomic and genomic mechanisms. Kidney Int 56:1400–1412
16. Karmazyn M, Liu Q, Gan XT, Brix BJ, Fliegel L 2003 Aldosterone increases NHE-1 expression and induces NHE-1-dependent hypertrophy in neonatal rat ventricular myocytes. Hypertension 42:1171–1176
17. Dostal DE, Baker KM 1998 Angiotensin and endothelin: messengers that couple ventricular stretch to the Na^+/H^+ exchanger and cardiac hypertrophy. Circ Res 83:870–873
18. Engelhardt S, Hein L, Keller U, Klambt K, Lohse MJ 2002 Inhibition of Na^+/H^+ exchange prevents hypertrophy, fibrosis, and heart failure in β1-adrenergic receptor transgenic mice. Circ Res 90:814–819
19. Harada E, Nakagawa O, Yoshimura M, Harada M, Nakagawa M, Mizuno Y, Shimasaki Y, Nakayama M, Yasue H, Kuwahara K, Saito Y, Nakao K 1999 Effect of interleukin-1β on cardiac hypertrophy and production of natriuretic peptides in rat cardocyte culture. J Mol Cell Cardiol 31:1997–2006
20. Despa S, Islam MA, Pogwizd SM, Bers DM 2002 Intracellular $[Na^+]$ and Na^+ pump rate in rat and rabbit ventricular myocytes. J Physiol 539:133–143
21. Hoffman JF, Geibel JP 2005 Fluorescent imaging of Cl^- in Amphiuma red blood cells: how the nuclear exclusion of Cl^- affects the plasma membrane potential. Proc Natl Acad Sci USA 102:921–926
22. Kuwahara K, Saito Y, Harada M, Ishikawa M, Ogawa E, Miyamoto Y, Hamanaka I, Kamitani S, Kajiyama N, Takahashi N, Nakagawa O, Masuda I, Nakao K 1999 Involvement of cardiotrophin-1 in cardiac myocyte-nonmyocyte interactions during hypertrophy of rat cardiac myocytes in vitro. Circulation 100:1116–1124
23. Ito T, Yoshimura M, Nakamura S, Nakayama M, Shimasaki Y, Harada E, Mizuno Y, Yamamuro M, Harada M, Saito Y, Nakao K, Kurihara H, Yasue H, Ogawa H 2003 Inhibitory effect of natriuretic peptides on aldosterone synthase gene expression in cultured neonatal rat cardiocytes. Circulation 107:807–810
24. de Gasparo M, Joss U, Ramjoue HP, Whitebread SE, Haenni H, Schenkel L, Kraehenbuehl C, Biollaz M, Grob J, Schmidlin J 1987 Three new epoxyspirolactone derivatives: characterization in vivo and in vitro. J Pharmacol Exp Ther 240:650–656

25. Matsumoto Y, Yamamoto S, Suzuki Y, Tsuboi T, Terakawa S, Ohashi N, Umemura K 2004 Na^+/H^+ exchanger inhibitor, SM-20220, is protective against excitotoxicity in cultured cortical neurons. Stroke 35:185–190
26. Masereel B, Pochet L, Laeckmann D 2003 An overview of inhibitors of Na^+/H^+ exchanger. Eur J Med Chem 38:547–554
27. Gu JW, Anand V, Shek EW, Moore MC, Brady AL, Kelly WC, Adair TH 1998 Sodium induces hypertrophy of cultured myocardial myoblasts and vascular smooth muscle cells. Hypertension 31:1083–1087
28. McChesney MB, Collins JR, Lu D, Lu X, Torten J, Ashley RL, Cloyd MW, Miller CJ 1998 Occult systemic infection and persistent simian immunodeficiency virus (SIV)-specific CD4+-T-cell proliferative responses in rhesus macaques that were transiently viremic after intravaginal inoculation of SIV. J Virol 72:10029–10035
29. Kumar AP, Piedrafita FJ, Reynolds WF 2004 Peroxisome proliferator-activated receptor γ-ligands regulate myeloperoxidase expression in macrophages by an estrogen-dependent mechanism involving the −463GA promoter polymorphism. J Biol Chem 279:8300–8315
30. Losel RM, Feuring M, Falkenstein E, Wehling M 2002 Nongenomic effects of aldosterone: cellular aspects and clinical implications. Steroids 67:493–498
31. Michea L, Delpiano AM, Hitschfeld C, Lobos L, Lavandero S, Marusic ET 2005 Eplerenone blocks nongenomic effects of aldosterone on the Na^+/H^+ exchanger, intracellular Ca^{2+} levels, and vasoconstriction in mesenteric resistance vessels. Endocrinology 146:973–980
32. Alzamora R, Marusic ET, Gonzalez M, Michea L 2003 Nongenomic effect of aldosterone on Na^+/K^+-adenosine triphosphatase in arterial vessels. Endocrinology 144:1266–1272
33. Oberleithner H, Ludwig T, Riethmüller C, Hillebrand U, Albermann L, Schäfer C, Shahin V, Schillers H 2004 Human endothelium. Target for aldosterone. Hypertension 43:1–5
34. Yamamura H, Ugawa S, Ueda T, Nagao M, Shimada S 2004 Protons activate the δ-subunit of the epithelial Na^+ channel in humans. J Biol Chem 279:12529–12534
35. Charlemagne D, Mayoux E, Poyard M, Oliviero P, Geering K 1987 Identification of two isoforms of the catalytic subunit of Na^+/K^+-ATPase in myocytes from adult rat heart. J Biol Chem 262:8941–8943
36. Mihailidou AS, Bundgaard H, Mardini M, Hansen PS, Kjeldsen K, Rasmussen HH 2000 Hyperaldosteronemia in rabbits inhibits the cardiac sarcolemmal Na^+-K^+ pump. Circ Res 86:37–42
37. Takeda Y, Yoneda T, Demura M, Furukawa K, Miyamori I, Mabuchi H 2001 Effects of high sodium intake on cardiovascular aldosterone synthesis in stroke-prone spontaneously hypertensive rats. J Hypertens 19:635–659
38. Gomez-Sanchez EP, Ahmad N, Romero DG, Gomez-Sanchez CE 2004 Origin of aldosterone in the rat heart. Endocrinology 145:4796–802
39. Ye P, Kenyon CJ, Mackenzie SM, Jong AS, Miller C, Gray GA, Wallace A, Ryding AS, Mullins JJ, McBride MW, Graham D, Fraser R, Connell JM, Davies E 2005 The aldosterone synthase (CYP11B2) and 11β-hydroxylase (CYP11B1) genes are not expressed in the rat heart. Endocrinology 146:5287–5293
40. Silvestre JS, Robert V, Heymes C, Aupetit-Faisant B, Mouas C, Moalic JM, Swynghedauw B, Delcayre C 1998 Myocardial production of aldosterone and corticosterone in the rat. J Biol Chem 273:4883–4891
41. Mizuno Y, Yasue H, Yoshimura M, Harada E, Fujii H, Nakamura S, Yamamoto N, Ogawa H, Nakao K 2005 Adrenocorticotropic hormone is produced in the ventricle of patients with essential hypertension. J Hypertens 23:411–416
42. Bers DM, Barry WH, Despa S 2003 Intracellular Na^+ regulation in cardiac myocytes. Cardiovasc Res 57:897–912
43. Pitt B, Zannad F, Remme WJ, Cody R, Castaigne A, Perez A, Palensky J, Wittes J 1999 The effect of spironolactone on morbidity and mortality in patients with severe heart failure. N Engl J Med 341:709–717
44. Pitt B, Remme W, Zannad F 2003 Eplerenone, a selective aldosterone blocker, in patients with left ventricular dysfunction after myocardial infarction. N Engl J Med 348:1309–1321
45. Young M, Funder J 2003 Mineralocorticoid action and sodium-hydrogen exchange: studies in experimental cardiac fibrosis. Endocrinology 144:3848–3851
46. Young MJ, Funder JW 2002 Mineralocorticoid receptors and pathophysiological roles for aldosterone in the cardiovascular system. J Hypertens 20: 1465–1468
47. Rocha R, Martin-Berger CL, Yang P, Scherrer R, Delyani J, McMahon E 2002 Selective aldosterone blockade prevents angiotensin II/salt-induced vascular inflammation in the rat heart. Endocrinology 143:4828–4836
48. Oliver WJ, Cohen EL, Neel JV 1975 Blood pressure, sodium intake, and sodium related hormones in the Yanomamo Indians, a "no-salt" culture. Circulation 52:146–151
49. Vasan RS, Evans JC, Larson MG, Wilson PWF, Meigs J B, Rifai N, Benjamin EJ, Levy D 2004 Serum aldosterone and the incidence of hypertension in non-hypertensive persons. N Engl J Med 351:33–41

Endocrinology **is published monthly by The Endocrine Society (http://www.endo-society.org), the foremost professional society serving the endocrine community.**

Notch/Rbp-j signaling prevents premature endocrine and ductal cell differentiation in the pancreas

Junji Fujikura,[1] Kiminori Hosoda,[1,*] Hiroshi Iwakura,[1] Tsutomu Tomita,[1] Michio Noguchi,[1] Hiroaki Masuzaki,[1] Kenji Tanigaki,[2] Daisuke Yabe,[2] Tasuku Honjo,[2] and Kazuwa Nakao[1]

[1] Department of Medicine and Clinical Science, Kyoto University Graduate School of Medicine, 54 Shogoin-Kawahara-cho, Sakyo-ku, Kyoto 606-8507, Japan
[2] Department of Medical Chemistry, Kyoto University Graduate School of Medicine, Yoshida-Konoe-cho, Sakyo-ku, Kyoto 606-8501, Japan
*Correspondence: pekopaokuro@yahoo.co.jp

Summary

To investigate the precise role of Notch/Rbp-j signaling in the pancreas, we inactivated Rbp-j by crossing Rbp-j floxed mice with *Pdx.cre* or *Rip.cre* transgenic mice. The loss of Rbp-j at the initial stage of pancreatic development induced accelerated α and PP cell differentiation and a concomitant decrease in the number of Neurogenin3 (Ngn3)-positive cells at E11.5. Then at E15, elongated tubular structures expressing ductal cell markers were evident; however, differentiation of acinar and all types of endocrine cells were reduced. During later embryonic stages, compensatory acinar cell differentiation was observed. The resultant mice exhibited insulin-deficient diabetes with both endocrine and exocrine pancreatic hypoplasia. In contrast, the loss of Rbp-j specifically in β cells did not affect β cell number and function. Thus, our analyses indicate that Notch/Rbp-j signaling prevents premature differentiation of pancreatic progenitor cells into endocrine and ductal cells during early development of the pancreas.

Introduction

The pancreas plays a key role in the maintenance of nutritional homeostasis through its exocrine and endocrine functions. The acini and ducts form the exocrine pancreas that produces and transports digestive enzymes into the duodenum. Besides, there are five known endocrine cell types in the pancreas: glucagon-producing α cells, insulin-producing β cells, somatostatin-producing δ cells, pancreatic polypeptide (PP)-producing PP cells, and ghrelin-producing ε cells (Heller et al., 2005).

Notch signaling regulates various developmental processes, such as neurogenesis, somitogenesis, angiogenesis, and hematopoiesis (Ishibashi et al., 1995; Hrabé de Angelis et al., 1997; Xue et al., 1999; Han et al., 2002). Interaction of a Notch receptor with its ligand induces cleavage of the receptor's intracellular domain (Notch ICD), which translocates to the nucleus and binds to Rbp-j to induce the expression of Hes family transcriptional repressors (Kageyama and Ohtsuka, 1999). Rbp-j is a key mediator of Notch signaling because it is expressed ubiquitously and associates with all four types of Notch receptors (Kato et al., 1996). Various Notch-related genes are expressed in the developing pancreas (Lammert et al., 2000). However, multiple anomalies and early embryonic lethalities of mice with homozygous deletions of genes such as *Dll1*, *Notch1*, *Notch2*, *Jagged1*, *Rbp-j*, or *Hes1* limits assessment of the importance of Notch/Rbp-j signaling in the pancreas (Swiatek et al., 1994; Ishibashi et al., 1995; Oka et al., 1995; Hrabé de Angelis et al., 1997; Apelqvist et al., 1999; Hamada et al., 1999; Xue et al., 1999; Jensen et al., 2000a). Although excess α cell differentiation in the pancreas has been reported at around E10 in mice with a generalized KO of Dll1 or Hes1 (Apelqvist et al., 1999; Jensen et al., 2000a), because β cells start to expand at around E13 and their differentiation occurs independently of α cells (Jensen et al., 2000b), the influence of Notch signaling on β cells remains to be elucidated. To address this issue, we created mice with developmental stage-specific deletion of *Rbp-j* in the pancreas using the Cre/loxP-mediated DNA recombination system.

Results

Accelerated premature differentiation of α and PP cells but not of β, δ, and ε cells in pancreatic Rbp-j KO (PRKO) mice

By crossing floxed Rbp-j (*Rbp-j$^{f/f}$*, designated as F/F) mice with *Pdx.cre* mice, we generated pancreatic Rbp-j KO (*Rbp-j$^{f/f}$ Pdx.cre*, designated as PRKO) mice (Gu et al., 2002; Han et al., 2002; see the Supplemental Data available with this article online). The *Pdx.cre* mouse begins to recombine loxP sites in the pancreatic epithelium before E9.5 (Figure S1B). Notch signaling negatively regulates proneural basic helix-loop-helix (bHLH) factors through Hes activation (Kageyama and Ohtsuka, 1999). A unique proendocrine bHLH transcription factor, Ngn3, is required for the development of pancreatic endocrine lineages (Gradwohl et al., 2000; Gu et al., 2002). We observed a premature increase in the number of Ngn3$^+$ cells in the pancreatic buds of PRKO mice (Figure S2A). At E11.5, a few scattered α cells among the protruding epithelial cells of F/F mice were observed (Figures 1E and 1E′). In PRKO mice, the number of α and PP cells increased and they surrounded the pancreatic buds (Figures 1F, 1F′, 1J, and 1J′). However, β, δ, and ghrelin-producing cell differentiation was not enhanced in the mutants (Figures 1D, 1D′, 1H, 1H′, and S3B). The number of Ngn3$^+$ cells decreased in PRKO mice compared with control mice (Figures 1M–1N′ and S2B). The number of proliferating cells detected by phosphohistone H3 (pHH3) immunostaining was comparable between control and mutant mice (Figures 1O–1P′). No apoptotic cells were

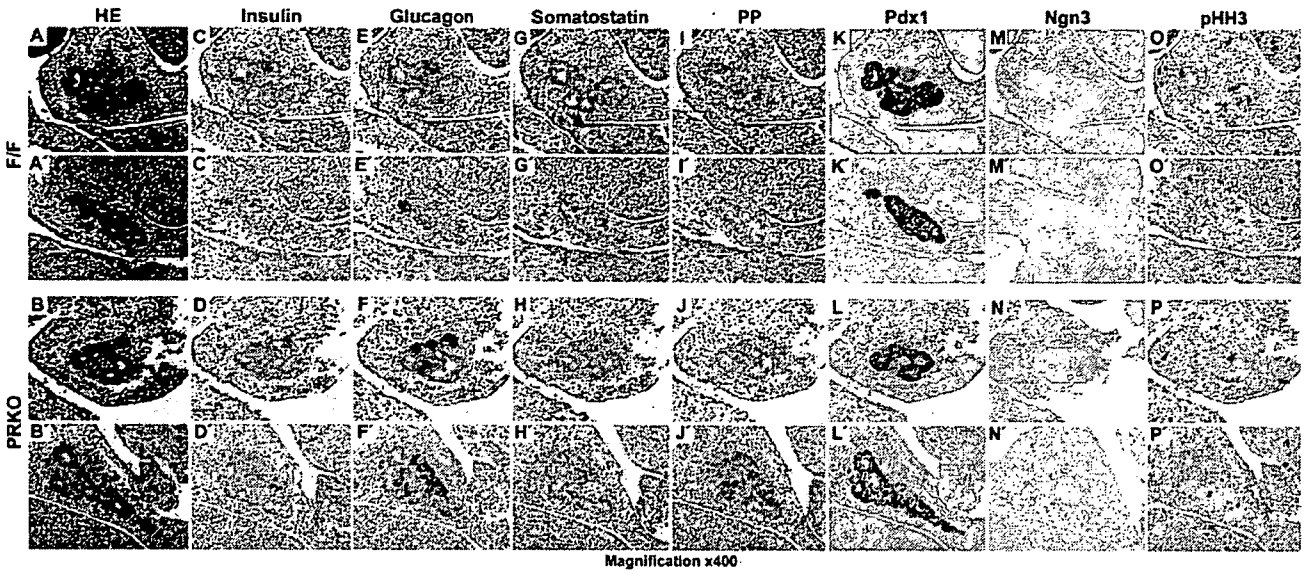

Figure 1. Accelerated premature differentiation of α and PP cells but not β, δ, and ε cells in pancreatic Rbp-j KO (PRKO) mice

A–P′) HE staining **(A–B′)**, and immunostaining **(C–P′)** of representative serial pancreatic sections from F/F mice and PRKO mice at E11.5.

detected in the pancreatic epithelia of control or mutant mice (Figures S3C–S3E). These data indicate that earlier commitment to proendocrine (Ngn3$^+$) cells induced by defective Notch signaling results in precocious endocrine cell differentiation and a substantial loss of proendocrine cells during early pancreatic development.

Elongated tubular structures with decreased branching morphogenesis in the pancreas of the PRKO mouse

At E15, pancreatic Pdx1$^+$ epithelium of control mice exhibited complex and ramified networks (Figure 2B). However, in the mutant, branching of Pdx1$^+$ epithelium was severely impaired, and dilated tubular structures were prominent (Figure 2B′). The decreased epithelial branching was not associated with increased cell death or decreased proliferation, because these cells were not apoptotic (Figure 2D′), but exhibited active division (Figure 2M′). Moreover, acinar and β cells were scarcely differentiated (Figures 2C′ and 2H′), and aggregated α cells existed around the columnar tubular epithelium (Figure 2G′). The cells lining the lumens of tubular structures showed positive staining with cytokeratin (CK) and Dolichos biflorus agglutinin (DBA) lectin (Dor et al., 2004) (Figures 2K–2L′). The glucose transporter 2 (Glut2), expressed on the surface of differentiated β cells (Figure 2N), is also thought to be a marker of early pancreatic progenitor cells (Pang et al., 1994); however, Glut2 was not expressed in the tubular epithelium (Figure 2N′). In the control pancreas, *Hes1* expression was not detected (Figure 2O), but scattered Ngn3$^+$ cells were evident at this stage (Figure 2P). In the mutant pancreas, expression of *Hes1* and Ngn3 was virtually absent (Figures 2O′ and 2P′). ISL1 is a LIM homeodomain protein whose expression is initiated after Ngn3 extinction but before hormone production (Ahlgren et al., 1997). ISL1 expression was not detected in the tubular epithelium (Figure 2Q′). This analysis of various differentiation markers shows that the cells lining these tubular structures are not early progenitors, nor are they on the endocrine lineage. The tubular morphologies and high columnar epithelium resembling that of the large pancreatic duct rather suggest that the cells positive for ductal markers are duct cells. We confirmed that all of these cells were derived from Rbp-j-deficient cells by lineage tracing (Figure S4).

At later embryonic stages of PRKO mice, the acinar cell area was much smaller and CK$^+$ ductal cells occupied a larger area compared with F/F mice (Figures S5A–S5F). Although compensatory acinar growth was observed (Figures S5E–S5H), the interval sections revealed a much smaller pancreas in the mutant than in the control mouse (Figure S5I).

PRKO mice are born with pancreatic hypoplasia and exhibit insulin-deficient diabetes

The adult PRKO mouse exhibited a small pancreas (Figure 3A). The absolute pancreatic weight (PRKO, 209 ± 73 mg versus F/F, 685 ± 81 mg; $p = 0.0038$; Figure 3B) and the ratio of pancreatic weight to total body weight (data not shown) were lower in PRKO mice than in F/F mice. In pancreatic sections from PRKO mice, the number of islets per pancreas area was reduced (PRKO, 0.15 ± 0.06 versus F/F, 0.62 ± 0.13 islets/mm^2; $p = 0.015$; Figures 3C and 3D), and the size of the islets was smaller compared with F/F mice (Figure 3C). The relative endocrine cell mass was quantified by estimating the hormone-positive area per total pancreatic area in multiple pancreatic sections. The β cell mass of the PRKO mice was markedly reduced to about 25% of the β cell mass of F/F mice (PRKO, 0.21 ± 0.08% versus F/F, 1.13 ± 0.04%; $p < 0.001$; Figure 3E), and the absolute α cell mass was also significantly reduced to about 50% of that of the F/F mice (PRKO, 0.11 ± 0.02% versus F/F, 0.24 ± 0.02%; $p < 0.001$; Figure 3E). Total pancreatic insulin content (expressed per mg of pancreas weight) estimated from an acid-ethanol extract of the whole pancreas. PRKO mice had much lower insulin contents

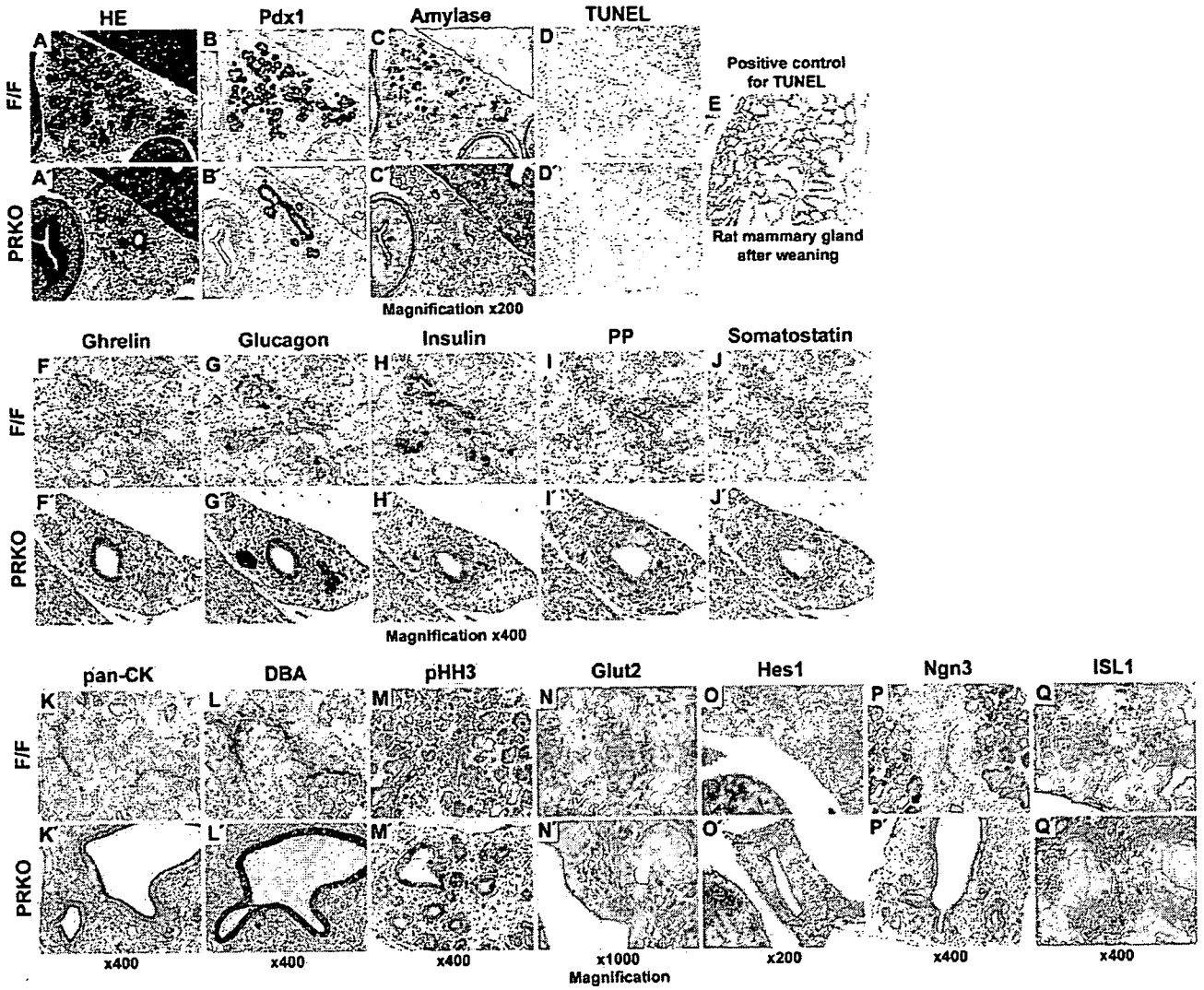

Figure 2. Elongated tubular structures with decreased branching in PRKO mice at E15

A–J') Dilated and elongated duct-like structures in PRKO mice. HE staining (A and A'), immunostaining (B–C' and F–J'), and TUNEL assay (D and D') of serial pancreatic sections from F/F mice and PRKO mice at E15. The mammary gland of a postlactating female Wistar rat was used as a positive control for apoptosis (E).

K–Q') Characterization of duct-like cells in PRKO mice. Immunostaining (K–N', P–Q') and *Hes1* in situ hybridization (O and O') of pancreatic sections from F/F and PRKO mice at E15.

than the F/F mice (PRKO, 0.9 ± 0.2 pg/mg pancreas versus F/F, 96.4 ± 9.9 pg/mg pancreas; $p < 0.001$; Figure 3F). In addition to the scarcity of islets, histological analysis of the adult pancreas in PRKO mice revealed that the endocrine cells were frequently observed in association with distended pancreatic ducts (Figures 3J, 3L, 3N, 3P, and 3R). The relative ductal hyperplasia observed during the embryonic stages of PRKO mice (Figure S5D) became obscured in adult PRKO mice (Figure 3C).

The growth of PRKO mice and F/F mice fed normal chow was observed for four months. PRKO mice had a leaner phenotype than F/F mice and exhibited no further weight gain (Figures 3S and 3T). At eight weeks of age, PRKO mice developed significant hyperglycemia during fasting and feeding (fasting—PRKO, 348 ± 61 mg/dl versus F/F, 98 ± 6 mg/dl; $p < 0.001$; morning fed—PRKO, 524 ± 59 mg/dl versus F/F, 124 ± 12 mg/dl; $p < 0.001$; Figure 3U), which was accompanied by notably decreased plasma insulin concentrations (fasting—PRKO, below detection limit versus F/F, 0.48 ± 0.07 ng/ml; $p < 0.001$; morning fed—PRKO 0.04 ± 0.03 ng/ml versus F/F, 1.35 ± 0.25 ng/ml; $p = 0.0013$; Figure 3V). At this age, the mutant mice showed polyuria and polydipsia, and some appeared lethargic. Daily food intake increased in PRKO mice compared with control mice (PRKO, 8.3 ± 0.6 g/24 hr versus F/F, 4.1 ± 0.3 g/24 hr; $p < 0.001$; Figure 3W), which corresponded to diabetic hyperphagia. Thus, PRKO mice exhibited characteristics typical of diabetes with defective insulin secretion. Furthermore, PRKO mice had lower serum amylase activities than F/F mice (PRKO, 711 ± 58 U/dl versus F/F, 1121 ± 67 U/dl; $p = 0.0015$; Figure 3X), presumably due to pancreatic hypoplasia and severe diabetes.

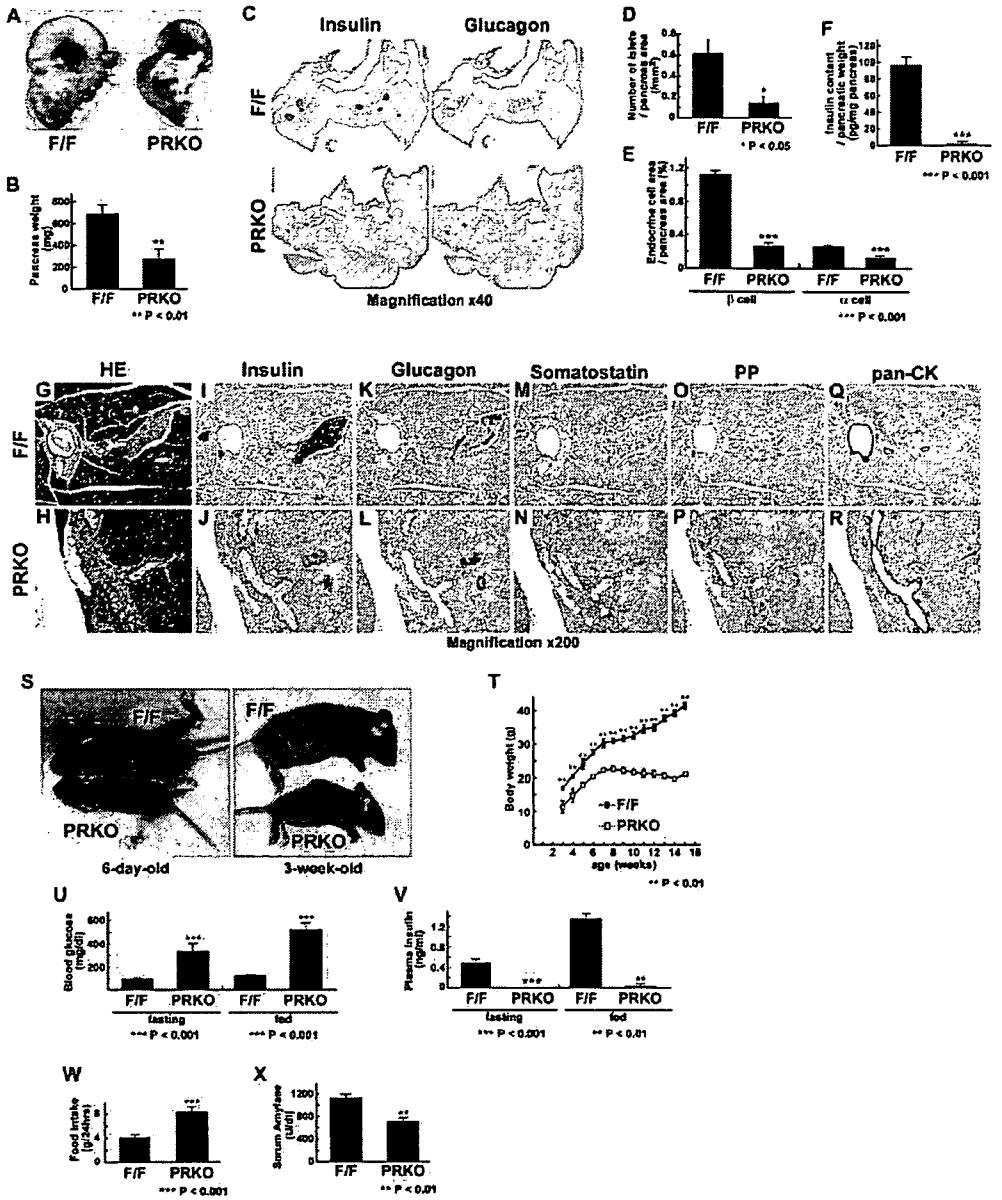

Figure 3. The adult PRKO mouse has a small pancreas, few islets, and low insulin content, which result in overt diabetes

A and B) Small pancreas in an adult PRKO mouse. Gut regions were dissected **(A)**, and pancreatic weights were measured at 12 weeks of age **(B)**.

C–E) Fewer islets and reduced endocrine cell mass in PRKO mice. Pancreatic sections from 10-week-old F/F mice and PRKO mice were immunostained for insulin and glucagon **(C)** to determine the number of islets **(D)**, β cell area **(E)**, and α cell area **(E)**, which were normalized to total pancreatic area.

F) Lower pancreatic insulin content in PRKO mice. Pancreatic insulin content was measured in acid-ethanol extracts from 6-week-old F/F mice and PRKO mice.

G–R) Duct-associated endocrine cells in PRKO mice. HE staining **(G and H)** and immunostaining **(I–R)** of serial pancreatic sections from 8-week-old F/F and PRKO mice. The number of β cells was markedly reduced **(J)**. Endocrine cells are located close to ductal structures **(J, L, N, and P)**.

S and T) Growth retardation in PRKO mice. Gross appearances **(S)** of 6-day-old (left) and 3-week-old (right) PRKO mice (bottom) and control littermates (top). Growth curve **(T)** for litters obtained from mating F/F mice and PRKO mice.

U–W) Insulin-deficient diabetes in PRKO mice. Blood glucose concentrations **(U)** and plasma insulin concentrations **(V)** from fasted and random-fed 8-week-old male F/F mice and PRKO mice. Food intake **(W)** was measured for 24 hr from 16-week-old male F/F mice and PRKO mice.

X) Exocrine pancreatic insufficiency in F/F *Rip.cre* mice. Amylase activity was measured in serum from F/F mice and PRKO mice at 10 weeks of age.

Bars represent means ± SE of n = 4–8 mice. Levels of significance (Student's t test) are shown (*p < 0.05; **p < 0.01; ***p< 0.001).

β cell-specific Rbp-j KO (βRKO) mice have normal β cell number and function

By crossing F/F mice with *Rip.cre* mice, we next generated β cell-specific Rbp-j KO (*Rbp-j$^{f/f}$ Rip.cre*, designated as βRKO) mice (Figure S6). βRKO mice had normal body weight (βRKO, 35.2 ± 2.6 mg/dl versus *Rip.cre*, 37.0 ± 2.5 mg/dl; p = 0.62; Figure 4A). No significant differences were detected in the levels of blood glucose (βRKO, 160 ± 17 mg/dl versus *Rip.cre*,

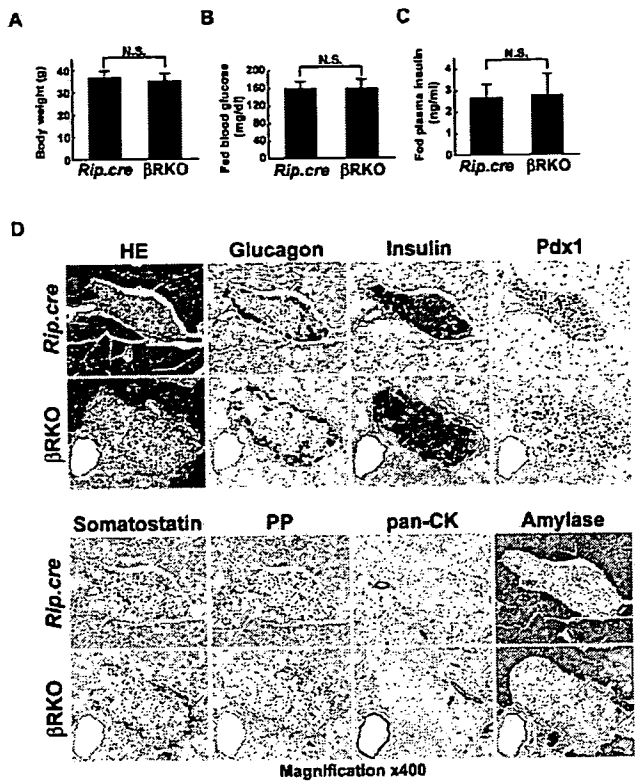

Figure 4. Absence of abnormalities in β cell-specific *Rbp-j* KO mice

A–C) Metabolic parameters of βRKO mice. Body weight (B), random-fed blood glucose concentrations (C), and random-fed plasma insulin concentrations (D) of 19-week-old male *Rip.cre* mice and βRKO mice.

D) Absence of morphological changes in the pancreas of the βRKO mouse. Immunohistochemistry of serial pancreatic sections of 20-week-old *Rip.cre* mice and βRKO mice.

Bars represent means ± SE of n = 7–8 mice. Levels of significance (Student's t test) are shown (NS, not significant).

159 ± 15 mg/dl; p = 0.95; Figure 4B) or plasma insulin (βRKO, 2.78 ± 1.10 ng/ml versus *Rip.cre*, 2.67 ± 0.55 ng/ml; p = 0.92; Figure 4C) in the fed state. Hematoxylin-eosin (HE) staining and immunohistochemical studies with glucagon, insulin, Pdx1, somatostatin, PP, pan-CK, and amylase revealed no abnormalities (Figure 4D). These data indicate that Rbp-j is not required for maintaining β cell function or β cell mass.

Discussion

Using the stage-specific conditional gene targeting approach, we documented the effects of Notch/Rbp-j signaling on pancreatic development and function.

Normally, Ngn3 expression peaks between E13.5 and E15.5 (Apelqvist et al., 1999). In PRKO mice, Ngn3 expression peaked at E10.5 and then declined at E11.5 (Figure 1), which suggests that termination of Notch signaling results in earlier commitment to endocrine cell lineages and earlier loss of endocrine progenitor cells. Before E12.5, the majority of endocrine cells formed are α and PP cells, and a wave of β and δ cell generation occurs after E13 (Pictet and Rutter, 1972; Murtaugh and Melton, 2003). In PRKO mice, α and PP cell differentiation was enhanced at E11.5, but β and δ cell differentiation was not enhanced. It was recently reported that Ngn3 protein transduction to E11.5 pancreatic cells resulted in α cell differentiation, but the transduction to E15 cells resulted in β cell differentiation (Dominguez-Bendala et al., 2005). In agreement with that report, our findings suggest that E11 proendocrine cells may lack some factor that contributes to β or δ cell differentiation.

Tubular structures with CK^+ DBA^+ cells dominated in the pancreas of the PRKO mouse at later embryonic stages (Figure 2). Thus, residual $Pdx1^+$ epithelial cells that have not undergone endocrine cell differentiation have a tendency to differentiate into ductal cells. A study demonstrated that genes that participate in the Notch pathway are upregulated in the metaplastic ductal epithelium of pancreatic premalignant legions (Miyamoto et al., 2003). Lineage-tracing studies show that ductal lineage is separated from $Pdx1^+$ $Ngn3^-$ common pancreatic progenitor cells between E9.5 and E12.5 (Gu et al., 2002); those are the times when the disruption of *Rbp-j* genes in PRKO mice occurs. These findings suggest that the appropriate downregulation of Notch signaling is necessary for pancreatic duct cell identity.

In the mutant mouse, the number of Pdx1-positive cells clearly decreased before E15 and the pancreas was small thereafter (Figures 2B′, 3A, and 3B). If the role of Notch signaling is simply to regulate cell fate, hypoplasia of certain types of cell should be accompanied by hyperplasia of other types of cell. For instance, in the determination of T and B lymphocytes, loss of function of Notch1 resulted in blockade of T cell development and enhancement of B cell production, while overexpression of Notch1 resulted in blockade of B cell lymphopoiesis and the generation of T cells (Pui et al., 1999; Wilson et al., 2001). The small pancreas and altered pancreatic cell composition in our mutant mouse suggest that defective Notch signaling allows premature differentiation of α, PP, and duct cells at the expense of later differentiating β, δ, and acinar cells. This mode of regulation is reminiscent of neuronal differentiation, in which Notch/Rbp-j signaling acts as a gatekeeper between self-renewal and commitment (Ishibashi et al., 1995).

In PRKO mice, though inadequate, the differentiation and growth of acinar cells occurred after E15. Persistent Notch ICD expression in pancreatic epithelium has been shown to inhibit acinar cell differentiation (Hald et al., 2003; Esni et al., 2004), and generalized Hes1 KO mice showed increased acinar cell growth (Jensen et al., 2000a). These results also suggest that Notch signaling inhibits acinar cell differentiation and proliferation during later embryonic stages.

The role of Notch signaling in terminally differentiated cells is unknown, although it was speculated that Notch might confer some degree of plasticity on postmitotic neurons (Ahmad et al., 1995). We detected the expression of Notch2 and Dll1 in endocrine cells of adult mice (data not shown). Furthermore, $Ngn3^+$ endocrine progenitor cells were shown to reside within the pancreatic islets (Gu et al., 2002); however, we found no difference between βRKO mice and control mice (Figure 4). It was reported that the β cells in adult islets are mainly formed by self-duplication of preexisting β cells and that the forced expression of Notch1 ICD in the adult pancreas does not perturb mature endocrine cells (Murtaugh et al., 2003; Dor et al., 2004). Together with the results of PRKO mice, Notch signaling may be indispensable only during the early developmental stages of the pancreas.

Our data show that Rbp-j is a key molecule in the propagation of pancreatic progenitor cells and is essential for proper differentiation into mature pancreatic cells.

Experimental procedures

Generation of pancreas- or β cell-specific Rbp-j KO mice

The generations of mice bearing a floxed allele of *Rbp-j* have been described previously (Han et al., 2002). *Pdx.cre* mice in which Cre recombinase is under the transcriptional control of the mouse Pdx1 promoter were gifts from Dr. Douglas A. Melton (Gu et al., 2002). *Rip.cre* mice in which Cre recombinase is under the control of the rat insulin II promoter were purchased from the Jackson Laboratory. Mice homozygous for the floxed *Rbp-j* allele (F/F) were crossed with *Pdx.cre* or *Rip.cre* transgenic mice. The resultant double-heterozygous mice were then crossed with *Rbp-j*$^{f/+}$ mice, resulting in *Rbp-j*$^{f/f}$ *Pdx.cre* (PRKO) or *Rbp-j*$^{f/f}$ *Rip.cre* (βRKO) mice and their control littermates. Genotyping and assessment of deletion efficiency were performed by Southern blot analyses on genomic DNA obtained from tails or other tissues.

Histological analyses

Whole embryos or excised pancreas were fixed with 4% paraformaldehyde in PBS for overnight at 4°C then paraffin embedded, and 5 μm sections were cut and mounted on glass slides. Slides were dewaxed, rehydrated, and, in some instances, subjected to antigen retrieval by autoclaving at 121°C for five minutes with 10 mM citrate buffer. Endogenous peroxidase was inactivated with 0.3% H_2O_2 in methanol for 30 min. The slides were blocked for 1 hr with a reagent containing casein (DAKO Protein Block Serum-Free Solution; Dako), then stained overnight with the following primary antibodies (Abs): rabbit anti-Pdx1 (Guz et al., 1995), rabbit anti-Hes1 (Jensen et al., 2000a), rabbit anti-Ngn3 (Schwitzgebel et al., 2000), guinea pig anti-Insulin (Dako), rabbit anti-Glucagon (Dako), rabbit anti-Somatostatin (Dako), rabbit anti-PP (Dako), rabbit anti-Ghrelin (Kojima et al., 1999), rabbit anti-pHH3 (Cell Signaling Technology), rabbit anti-pan-CK (Santa Cruz), rabbit anti-Amylase (Sigma-Aldrich), rabbit anti-Glut2 (Thorens et al., 1992), mouse anti-ISL1 (Developmental Studies Hybridoma Bank). The slides were washed with PBS the following day and incubated for 2 hr with the following secondary antibodies: biotinylated goat anti-guinea pig IgG; biotinylated goat anti-rabbit IgG, and biotinylated rabbit anti-goat IgG (all from Vector). The slides were then incubated with avidin-biotin complex (ABC) reagent (Vectastain Elite ABC Kit; Vector) for 50 min followed by the addition of diaminobenzidine tetrahydrochloride (DAB) (Dako) as a substrate-chromogen solution. After hematoxylin counterstaining and dehydration, slides were mounted in mounting medium (MGK-S; Matsunami) and pictures were taken using an Axioskop Microscope (Carl Zeiss). Morphometric analyses of pancreas were carried out using the Scion Image analysis program (Scion). The number of islets was calculated, with the definition of an islet as a group of endocrine cells containing at least five visible nuclei. The endocrine cell mass was calculated as the ratio of each hormone-positive cell area to the total area of the pancreas section. An In situ Apoptosis Detection Kit (Takara) was used for TUNEL (terminal deoxynucleotidyl transferase-mediated dUTP nick end labeling) assays, and tissue taken from the involuting mammary gland of a post-lactating female Wistar rat was used as a positive control for apoptosis. Counterstaining of these sections was performed with methyl green. For E15 embryos, in situ hybridization of *Hes1* was carried out using digoxigenin-labeled cRNA probes according to the reported protocol (Tomita et al., 2000).

Analysis of metabolic parameters

Blood glucose values were determined from whole venous blood taken from mouse tails using an automatic glucometer (Glutest Ace, Sanwa Kagaku) or an enzyme colorimetric assay kit (Glucose CII test, Wako). Blood for insulin and amylase was taken by retroorbital bleeds. Plasma insulin levels were measured using an ELISA kit (Morinaga). For glucagon, blood samples were collected into tubes containing EDTA (1 mg/ml blood) and aprotinin (500 KIE/ml blood). For measurements of pancreatic insulin contents, pancreas were quickly dissected, weighed, and frozen in liquid nitrogen. Insulin was extracted by mechanical homogenization in iced acid ethanol. After 24 hr at 4°C, samples were centrifuged, and the supernatant was collected and stored at −20°C. Insulin concentrations were determined by ELISA. Amylase activity was measured according to the Caraway method using a kit (Amylase-Test Wako, Wako). All values are expressed as mean ± standard error.

Supplemental data

Supplemental Data include six figures, Supplemental Results, and Supplemental Experimental Procedures and can be found with this article online at http://www.cellmetabolism.org/cgi/content/full/3/1/59/DC1/.

Acknowledgments

We thank Dr. Douglas A. Melton for providing *Pdx.cre* mice, Dr. Christopher V.E. Wright for anti-Pdx1 Ab, Dr. Michael S. German for anti-Ngn3 Ab, Dr. Bernard Thorens for anti-Glut2 Ab, Dr. Kenji Kangawa for anti-Ghrelin Ab, and Ryoichiro Kageyama for anti-Hes1 Ab. This work was supported by research grants from the Japanese Ministry of Education, Culture, Sports, Science, and Technology and the Japanese Ministry of Health, Labor and Welfare.

Received: August 2, 2005
Revised: October 30, 2005
Accepted: December 16, 2005
Published: January 10, 2006

References

Ahlgren, U., Pfaff, S.L., Jessell, T.M., Edlund, T., and Edlund, H. (1997). Independent requirement for ISL1 in formation of pancreatic mesenchyme and islet cells. Nature *385*, 257–260.

Ahmad, I., Zaqouras, P., and Artavanis-Tsakonas, S. (1995). Involvement of Notch-1 in mammalian retinal neurogenesis: association of Notch-1 activity with both immature and terminally differentiated cells. Mech. Dev. *53*, 73–85.

Apelqvist, A., Li, H., Sommer, L., Beatus, P., Anderson, D.J., Honjo, T., Hrabe de Angelis, M., Lendahl, U., and Edlund, H. (1999). Notch signalling controls pancreatic cell differentiation. Nature *400*, 877–881.

Dominguez-Bendala, J., Klein, D., Ribeiro, M., Ricordi, C., Inverardi, L., Pastori, R., and Edlund, H. (2005). TAT-mediated neurogenin 3 protein transduction stimulates pancreatic endocrine differentiation in vitro. Diabetes *54*, 720–726.

Dor, Y., Brown, J., Martinez, O.I., and Melton, D.A. (2004). Adult pancreatic beta-cells are formed by self-duplication rather than stem-cell differentiation. Nature *429*, 41–46.

Esni, F., Ghosh, B., Biankin, A.V., Lin, J.W., Albert, M.A., Yu, X., MacDonald, R.J., Civin, C.I., Real, F.X., Pack, M.A., et al. (2004). Notch inhibits Ptf1 function and acinar cell differentiation in developing mouse and zebrafish pancreas. Development *131*, 4213–4224.

Gradwohl, G., Dierich, A., LeMeur, M., and Guillemot, F. (2000). Neurogenin3 is required for the development of the four endocrine cell lineages of the pancreas. Proc. Natl. Acad. Sci. USA *97*, 1607–1611.

Gu, G., Dubauskaite, J., and Melton, D.A. (2002). Direct evidence for the pancreatic lineage: NGN3+ cells are islet progenitors and are distinct from duct progenitors. Development *129*, 2447–2457.

Guz, Y., Montminy, M.R., Stein, R., Leonard, J., Gamer, L.W., Wright, C.V.E., and Teitelman, G. (1995). Expression of murine STF-1, a putative insulin gene transcription factor, in β cells of pancreas, duodenal epithelium and pancreatic exocrine and endocrine progenitors during ontogeny. Development *121*, 11–18.

Hald, J., Hjorth, J.P., German, M.S., Madsen, O.D., Serup, P., and Jensen, J. (2003). Activated Notch1 prevents differentiation of pancreatic acinar cells and attenuate endocrine development. Dev. Biol. *260*, 426–437.

Hamada, Y., Kadokawa, Y., Okabe, M., Ikawa, M., Coleman, J.R., and Tsujimoto, Y. (1999). Mutation in ankyrin repeats of the mouse Notch2 gene induces early embryonic lethality. Development *126*, 3415–3424.